



Mineralogy of the Venus Surface

Martha S. Gilmore¹ · M. Darby Dyar^{2,3} · Nils Mueller⁴ · Jérémy Brossier⁵ · Alison R. Santos¹ · Mikhail Ivanov⁶ · Richard Ghail⁷ · Justin Filiberto⁸ · Jörn Helbert⁴

Received: 27 February 2023 / Accepted: 11 July 2023
© The Author(s) 2023

Abstract

Surface mineralogy records the primary composition, climate history and the geochemical cycling between the surface and atmosphere. We have not yet directly measured mineralogy on the Venus surface in situ, but a variety of independent investigations yield a basic understanding of surface composition and weathering reactions in the present era where rocks react under a supercritical atmosphere dominated by CO₂, N₂ and SO₂ at ~460 °C and 92 bars. The primary composition of the volcanic plains that cover ~80% of the surface is inferred to be basaltic, as measured by the 7 Venera and Vega landers and consistent with morphology. These landers also recorded elevated SO₃ values, low rock densities and spectral signatures of hematite consistent with chemical weathering under an oxidizing environment. Thermodynamic modeling and laboratory experiments under present day atmospheric conditions predict and demonstrate reactions where Fe, Ca, Na in rocks react primarily with S species to form sulfates, sulfides and oxides. Variations in surface emissivity at ~1 μm detected by the VIRTIS instrument on the Venus Express orbiter are spatially correlated to geologic terrains. Laboratory measurements of the near-infrared (NIR) emissivity of geologic materials at Venus surface temperatures confirms theoretical predictions that 1 μm emissivity is directly related to Fe²⁺ content in minerals. These data reveal regions of high emissivity that may indicate unweathered and recently erupted basalts and low emissivity associated with tessera terrain that may indicate felsic materials formed during a more clement era. Magellan radar emissivity also constrain mineralogy as this parameter is inversely related to the type and volume of high dielectric minerals, likely to have formed due to surface/atmosphere reactions. The observation of both viscous and low viscosity volcanic flows in Magellan images may also be related to composition. The global NIR emissivity and high-resolution radar and topography collected by the VERITAS, EnVision and DAVINCI missions will provide a revolutionary advancement of these methods and our understanding of Venus mineralogy. Critically, these datasets must be supported with both laboratory experiments to constrain the style and rate weathering reactions and laboratory measurements of their NIR emissivity and radar characteristics at Venus conditions.

Keywords Venus · Mineralogy · Spectroscopy

Venus: Evolution Through Time

Edited by Colin F. Wilson, Doris Breuer, Cédric Gillmann, Suzanne E. Smrekar, Tilman Spohn and Thomas Widemann

Extended author information available on the last page of the article

1 Introduction

Mineralogy is key to understanding the geologic and climate evolution of all terrestrial planets. The mineralogical analysis of meteorites, returned samples and in situ measurements for the Moon, Mars and some asteroids form the basis of our understanding of the bulk composition of the solar system and the influence of water over the history of these bodies. For airless bodies and those with thinner atmospheres, mineralogy can be assessed from orbit using spectroscopy in the visible to thermal wavelengths, however the massive atmosphere of Venus prohibits hyperspectral imaging from orbit in these wavelengths.

Meadows and Crisp (1996) observed the nightside of Venus from Earth and identified 5 spectral windows between 1.00–1.31 μm in the near infrared (NIR) where radiance from the surface can be detected above the Venus atmosphere. These windows were exploited by the Cassini Visible and Infrared Mapping Spectrometer (VIMS) instrument (Baines et al. 2000), the Galileo Near Infrared Mapping Spectrometer (NIMS) instrument (Hashimoto et al. 2008) and the Parker Solar Probe Wide-Field Imager for Solar Probe (WISPR) instrument (Wood et al. 2022) during Venus flybys. Hashimoto et al. (2008) showed that recognizable surface features were visible from orbit at 1.18 μm and developed a methodology to use other channels to correct for the influence of the atmosphere in the surface emissivity data. Because the ~ 1 μm spectral region is sensitive to FeO content in minerals, these data can be used to constrain global surface composition (Dyar et al. 2020). Hashimoto and Sugita (2003) calculated that NIR radiance differences could be related to variations in mineralogy. The Visible and Infrared Thermal Imaging Spectrometer (VIRTIS) instrument on Venus Express (VEx) mapped the NIR radiance of the southern hemisphere of Venus, and demonstrated that radiance anomalies correlate to geological features mapped by Magellan where variations can be plausibly related to mineralogy derived from thermodynamic modeling of the primary composition and weathering reactions at the Venus surface (Mueller et al. 2008; Helbert et al. 2008; Smrekar et al. 2010). These inferences are supported by recent laboratory measurements of rocks and minerals at Venus temperatures that confirm a relationship between FeO content and ~ 1 μm emissivity (Dyar et al. 2020; Helbert et al. 2021). These observations are the basis for the design of the Venus Emissivity Mapper (VEM) instrument on NASA's Venus Emissivity, Radio science, InSAR, Topography, And Spectroscopy (VERITAS) mission (Helbert et al. 2020), the Venus Imaging System for Observational Reconnaissance (VISOR) and Venus Descent Imager (VenDI) instruments on NASA's Deep Atmosphere Venus Investigation of Noble gases, Chemistry, and Imaging (DAVINCI) mission (Garvin et al. 2022) and the VenSpec-M imaging system on ESA's EnVision mission (Widemann et al. 2021), which will for the first time provide maps of the global distribution of ~ 1 μm emissivity from orbit and at a single site below the clouds.

On the eve of these revolutionary measurements, we summarize the current understanding of the mineralogy of Venus.

2 Theory

2.1 NIR Emissivity

Spectral windows permit the observation of Venus surface thermal emission through the cloud deck. Surface thermal emission has been detected in windows within the wavelength range of 0.7 to 1.2 μm (Lecacheux et al. 1993; Meadows and Crisp 1996; Baines et al. 2000; Wood et al. 2022). Surface thermal emission can be described by the product of

Planck-function of the surface temperature and surface emissivity, which is indicative of surface composition. The radiation from the surface is modified during its transfer through the atmosphere by scattering, absorption, and emission by atmospheric gasses and aerosols. Thus, the derivation of emissivity from orbiter observations requires constraints on the surface temperature as well as on the variables going into the radiative transfer model used for atmospheric correction. The overall uncertainties of these parameters are large, so that an absolute emissivity cannot be derived with a useful uncertainty from single observations (Kappel et al. 2015). Some uncertainties of atmospheric variables such as the continuum absorption are large but affect all locations equally. Other error sources are related to cloud microphysics and can be assumed to be random errors at each time a location is observed. Taken together it is possible to average images of a specific region acquired at different times to reduce the uncertainty of the relative emissivity so that studies of surface composition are feasible (e.g., Dyar et al. 2020). In the following we try to highlight the most important open questions and limitations of deriving emissivity from orbiter observations.

The atmospheric transmittance within the spectral windows is dominated by the effect of scattering of molecules and cloud particles, with little absorption. This has two important consequences. First, the scattering randomizes the direction of photons so that the top-of-atmosphere radiance is a blurred image of the surface thermal emission. Moroz (2002) estimates that the blurring reduces the achievable spatial resolution to about two times the altitude of the cloud base, which is limited by the stability of H_2SO_4 to be above 45 km (Ragent et al. 1985). Hashimoto and Imamura (2001) and Basilevsky et al. (2012) ran Monte Carlo models of photon scattering and describe the effect of scattering as similar to convolution of the surface image with a Gaussian curve with a full width at half maximum of 90 and 100 km, respectively. There is so far no study that confirms this theoretical prediction. Kappel et al. (2015) note that the averaging of several images acquired by orbiters with a certain pointing uncertainty introduces an additional blurring effect. The achievable resolution of observations from below the cloud deck can be significantly higher as the fraction of photons only slightly deviating from the direct path is larger (Knically and Herrick 2020; Ekonomov 2015), although some reduction of the contrast from diffuse radiation is to be expected (Moroz 2002), and has to be corrected for in surface imaging studies.

The second important effect of scattering is that a significant amount of upwelling radiation is reflected downward, and thus illuminates the surface. Due to Kirchhoff's law this results in a non-linear relation of top-of-atmosphere radiance as function of surface emissivity, which reduces the sensitivity of the measurements to emissivity at high emissivity values (Hashimoto and Sugita 2003). Since the relation is non-linear, and the absolute emissivity cannot be strongly constrained, there is additionally an uncertainty in the amplitude of any observed emissivity differences. Smrekar et al. (2010) used the analytical approximation of this effect from Hashimoto and Sugita (2003) to estimate that the average emissivity of Venus is around 0.6 to maintain relatively high emissivity locations within a plausible range of less than 0.95. However, this approximation neglects the effect of gaseous absorption, and recent analyses of these data with numerical radiative transfer models shows much smaller emissivity differences on the order of a few percent (Kappel et al. 2016; Mueller et al. 2020). As discussed in the following, the atmospheric absorption itself is not well known. This highlights the importance of "ground truth" comparison of orbiter data to in situ data, such as that collected by the spectrophotometers on the Venera landers (Ekonomov et al. 1980; Helbert et al. 2021), which will be an extremely useful synergy for the VERITAS, DAVINCI and EnVision missions.

The gaseous absorption deep in the atmosphere of Venus at wavelengths far from absorption band centers is not well known. The deep atmosphere is far from an ideal gas, molecular

collisions are frequent, which results in a significant continuum of absorption (Pollack et al. 1993). Laboratory measurements of this continuum at both Venus near-surface temperature and pressure have not yet been achieved, although laboratory capabilities are approaching these conditions (Snels et al. 2021). The lack of constraints on this collision induced absorption (CIA) coefficient means that the average radiance observed at the cloud tops can correspond to a wide range of surface emissivity (Mueller et al. 2020). The CIA also has an effect on the gradient of radiance with respect to topography, and this has been used to constrain the CIA (Fedorova et al. 2015). This estimate however implies that the relation of surface temperature and topography is well known.

The surface is generally assumed to be very near to thermal equilibrium with the lowest atmosphere, due to the long solar day (243 Earth days), the high heat capacity of the atmosphere and the small insolation at the surface. The temperature of the lowest atmospheric layer is however not well known. Most studies aiming to derive surface emissivity from NIR radiances have relied on the temperature profile defined by the Venus International Reference Atmosphere (VIRA, Seiff et al. 1985). Most of the studies that use VIRA to derive emissivity find that there is a trend of the derived emissivity with topography (Meadows and Crisp 1996; Haus and Arnold 2010; Basilevsky et al. 2012; Kappel et al. 2016; Mueller et al. 2020). The trend is much more gradual than the trend observed in the radiothermal emissivity, and begins at lower elevations, indicating that there is not a common cause for these two phenomena. Meadows and Crisp (1996) instead propose that the lapse rate is different from the VIRA model.

The VIRA model is based mostly on the four Pioneer Venus descent probes, which provide temperature profiles from a wide range of local times and latitudes that converge to similar temperatures with increasing depth in the atmosphere. They however all experienced malfunctions around 18 km altitude. The temperatures in the VIRA model are extrapolated downwards and thus may not include any variation in the temperature lapse rate. The Vega 2 probe observed such variation (Seiff 1987) in the form of a layer between 2 and 7 km altitude, where the lapse rate exceeds that of the VIRA model. The lapse rate also exceeds the calculated adiabatic lapse rate, indicating an unstable stratification that is difficult to explain. The possibility of such a superadiabatic lapse rate is discussed as explanation for the low brightness temperature of Venus highlands observed by Galileo NIMS, but Hashimoto et al. (2008) reject this as impossible and instead interpret it as low emissivity highlands to have a more felsic composition. Lebonnois and Schubert (2017) more recently propose that the Vega profile can be explained by a chemical gradient in the lower atmosphere, i.e., that increasing density stabilizes the apparently superadiabatic layer. It is not clear yet what could cause such a chemical gradient, but it is becoming clearer that the structure and composition of the lower atmosphere may still surprise us when the DAVINCI probe will make its descent. Without better knowledge of the lowest atmosphere, it should be stressed that only robust interpretations are those that compare observed emissivity differences between areas of similar elevation and thus temperature. This approach is utilized by Gilmore et al. (2015) to show that the Alpha Regio tessera terrain has a lower emissivity than the volcanic plains of the adjacent Eve Corona in the same topography range. The close proximity of Alpha and Eve Corona also mitigate potential regional variations in surface temperature, further supporting a correlation between the low emissivity values and surface properties (Sect. 3.2.1).

Mueller et al. (2020) has shown that the apparent trend of derived emissivity with topography varies from region to region. The trend appears to be consistent in regions with scales on the order of 1000 km, so that emissivity variation on smaller scales can be interpreted by correcting for this trend. The causes for these trends are likely the temperatures in the planetary boundary layer and the effect of surface topography on atmospheric dynamics. Global

Circulation Models (GCM) by Lebonnois et al. (2018) show that the atmospheric temperatures show lateral temperature variations that are qualitatively consistent with the variations of the emissivity trend (Mueller et al. 2018). The GCM predicts slope winds associated with the topography of the two regions compared by Mueller et al. (2020): (1) Lavinia Planitia, surrounded on three sides by highlands, and (2) Themis Regio, a highland consisting of a broad swell and volcanic edifices surrounded by lowlands, that may provide a hint as to why there is a temperature difference that is not equilibrated by the expected efficient convection on Venus. This topic requires more research, specifically the systematic comparison of observed brightness temperatures and the surface temperatures predicted by GCM models. It should be stressed that the GCMs still predict that the temperature contrasts at night are small within the same region, so that local emissivity variation can be derived with high accuracy. If emissivity differences are to be derived globally, e.g., when comparing a global emissivity map to an in situ measurement, the lateral temperature differences may be larger on the order of 5 K, corresponding to an emissivity difference of about 10%.

2.2 Radar Emissivity

Radar is largely insensitive to surface mineralogy except for minerals with a high dielectric constant, e.g., pyrite, or metals (which have essentially infinite dielectric constants). Materials with a high dielectric constant are more efficient reflectors and poor emitters and will thus have a higher Fresnel reflectivity and lower emissivity. In active radar, the reflectivity and roughness both contribute to the radar backscatter cross section (Hagfors 1970), which can be measured by both radar imaging and radar altimeter modes, each of which have different sensitivities (e.g., Garvin et al. 1985; Pettengill et al. 1988). However, in many circumstances it can be difficult to disentangle the relative contributions of dielectric constant and roughness in radar brightness measurements.

Passive radiometry, in which the radar sensor simply receives the naturally emitted radio energy from the hot Venus surface, is also sensitive to the dielectric constant, where radiance is a function of emissivity and material temperature as determined from the Stefan-Boltzman equation. This method was first used from orbit by the Pioneer Venus (PV) radar mapper ($\lambda = 17$ cm; Ford and Pettengill 1983). Taking the surface temperatures and atmospheric lapse rates measured by the Venera landers and the PV probes, they recognized that low regions of radio brightness could not be due to temperature differences alone, and required surface materials of low radar emissivity. These anomalously low values were corroborated by observations from the Very Large Array (VLA; $\lambda = 20$ cm; Pettengill et al. 1988). The Magellan radar ($\lambda = 12.6$ cm), made the first global emissivity map of Venus, resampled to 4.5 km, and gives a mean global value of emissivity of 0.845 (Pettengill et al. 1992). Using the relative Magellan SAR backscatter brightness as a proxy for surface roughness to ratio between smooth and rough surfaces, the dielectric permittivity can be calculated from Magellan emissivity (Fig. 1). Campbell (1994) calculated empirically dependencies on Magellan emissivity, SAR (HH and VV) radar cross section and emission angle that allow a more accurate and comparable derivation of emissivity values between smooth (plains) and rough (tesserae, mountain belts, rifts) terrains.

The Magellan data agree with previous observations of regions with anomalously low microwave emissivity and thus high values (up to ~ 160) for dielectric permittivity of surface materials (Fig. 1). Geologically, these values require that the rocks contain minerals or phases with a high dielectric constant (=real part of the relative dielectric permittivity), where the observed value is a function of the composition, volume, dispersion, permittivity of the matrix, porosity, density, temperature, grain size and shape of the phases. Olhoeft

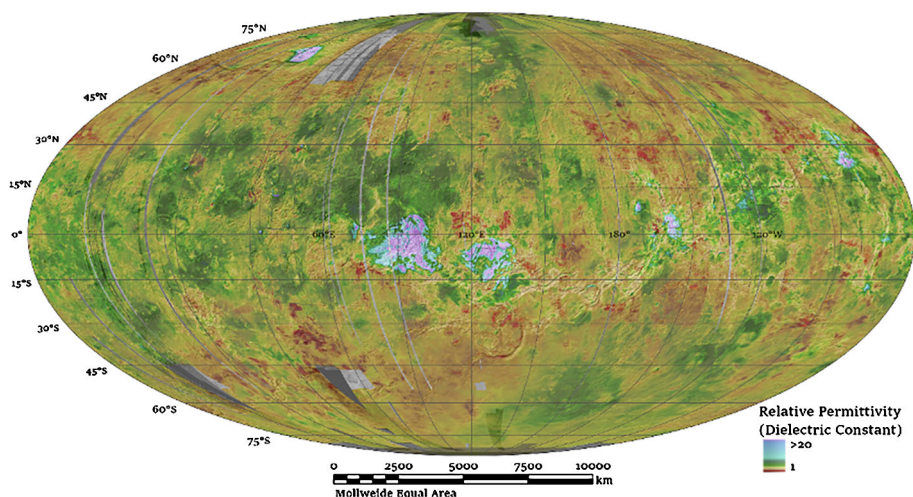


Fig. 1 Relative permittivity (dielectric constant) derived from Magellan emissivity, corrected for surface roughness inferred from SAR images. Red areas are low density unlithified materials, yellow areas are low density lithified materials, and green areas are medium to high density rocks. Blue and purple areas are high dielectric materials of unknown composition. See Sect. 3.3 for further discussion

and Strangway (1975) derived an empirical relationship between density and bulk dielectric constant of rocks and soils and show a dependence on Fe-Ti content of constituent minerals confirmed by others (e.g., Carrier et al. 1991). Shepard et al. (1994) show that the shape of the grains (e.g., needle-like, tabular, or spherical) can change the volume required by 3 orders of magnitude. The change in the crystal lattice with temperature has been shown to affect the dielectric constant (e.g., Havinga 1961; Roberts and Tyburczy 1991). Thus, perhaps most limiting to our ability to derive specific mineralogy from the dielectric permittivity data is the lack of systematic laboratory measurements of well-characterized (composition, density) Venus-relevant minerals at Venus temperatures and relevant radio frequencies.

The derivation of emissivity from radiance also depends strongly on the assumption of physical temperature of the material. As mentioned in the previous section, this depends on a limited number of direct measurements of the surface, the inferred change in lapse rate of atmospheric temperature and its relationship to topography. Also, as described in Pettengill et al. (1992), the brightness temperature as measured by the spacecraft is dependent on a number of factors, including properties of the radar antenna, the absorption and emission of the Venus atmosphere, and the estimate of the surface reflection of thermal energy from the sky. Better knowledge of the properties of the Venus atmosphere and topography by the upcoming missions will refine our measurements of radiothermal emission.

3 Observations

3.1 Venera Landers

To date, the only in situ direct measurements we have of Venus surface materials are from the Venera and Vega landers, which collected data from the surface of the planet in a period from 1972 (Venera 8) to 1985 (Vega 1,2). Chemical measurements of surface materials were made

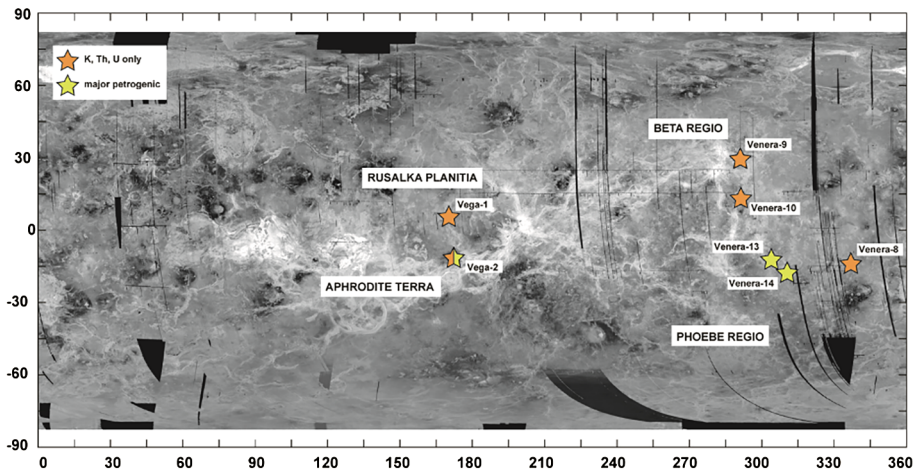


Fig. 2 Landing sites of the Soviet stations of the Venera-Vega series

Table 1 Gamma ray analyses conducted by the Venera and Vega landers. Concentrations are reported with 2σ uncertainty (Surkov et al. 1987; Treiman 2007), compared to averaged values for Mid Ocean Ridge Basalt (MORB) glass

Lander	K (%)	Th (ppm)	U (ppm)
Venera 8	4.0 ± 2.4	6.5 ± 0.4	2.2 ± 1.4
Venera 9	0.5 ± 0.2	3.7 ± 0.8	0.6 ± 0.4
Venera 10	0.3 ± 0.4	0.7 ± 0.6	0.5 ± 0.6
Vega 1	0.45 ± 0.44	1.5 ± 2.4	0.64 ± 0.94
Vega 2	0.40 ± 0.40	2.0 ± 2.0	0.68 ± 0.76
MORB Glass ^a	0.14 ± 0.15	0.4 ± 0.5	0.12 ± 0.14

^aAverage and standard deviation (2σ) of all reported values from 3190 samples in Table S2 of Le Voyer et al. (2019).

at seven locations that are concentrated in the Beta-Phoebe region and in Rusalka Planitia to the north of Aphrodite Terra (Kargel et al. 1993; Abdrakhimov and Basilevsky 2002; Fig. 2). Additionally, color photometry (Venera 9 and 10) and color images (Venera 13 and 14) of the surface yield some information about the surface mineralogy and oxidation state (Pieters et al. 1986). Selection of the landing sites was based purely on the interplanetary ballistic and communication constraints because no knowledge of the surface geology existed when the Venera-Vega missions were planned and implemented. Despite this formidable challenge, ten Soviet automatic landers successfully operated on the surface of Venus for periods of up to two hours, including the first soft landing of a spacecraft on the surface of another planet (Venera 7, 1970) and the first returned images from the surface of another planet (Venera 9, 1975).

The concentrations of K, Th, U were measured at five landing sites (Venera 8, 9, 10, Vega 1 and Vega 2) using gamma-ray spectrometry (Table 1; Surkov et al. 1987). The concentrations of the major petrogenic elements were measured at the sites of Vega 2, Venera 13, and 14 by X-ray fluorescence (XRF) (Table 2; Surkov et al. 1984, 1986). There is general consensus that the major element data are consistent with tholeiitic basalts at the Venera 14

Table 2 X-ray Fluorescence chemical analyses (wt%, (2 σ) conducted by the Venera and Vega landers, compared to averaged values for MORB glass

Oxide	Venera 13 ^a	Venera 14 ^a	Vega 2 ^b	MORB Glass ^c
SiO ₂	45.1 \pm 6.0	48.7 \pm 7.2	45.6 \pm 6.4	50.42 \pm 0.87
TiO ₂	1.59 \pm 0.9	1.25 \pm 0.82	0.2 \pm 0.2	1.47 \pm 0.38
Al ₂ O ₃	15.8 \pm 6.0	17.9 \pm 5.2	16 \pm 3.6	15.21 \pm 0.93
FeO	9.3 \pm 4.4	8.8 \pm 3.6	7.7 \pm 2.2 [*]	10.05 \pm 1.21
MnO	0.2 \pm 0.2	0.16 \pm 0.16	0.14 \pm 0.24	0.18 \pm 0.03
MgO	11.4 \pm 12.4	8.1 \pm 6.6	11.5 \pm 7.4	7.63 \pm 0.88
CaO	7.1 \pm 1.92	10.3 \pm 2.4	7.5 \pm 1.4	11.74 \pm 0.78
K ₂ O	4.0 \pm 1.26	0.2 \pm 0.14	0.1 \pm 0.16	0.17 \pm 0.17
SO ₃	1.62 \pm 2.0	0.88 \pm 1.54	4.7 \pm 3.0	0.37 \pm 0.05 [^]
Cl	<3000 ppm	<4000 ppm	<3000 ppm	182 \pm 279 ppm
Cu			<3000 ppm	79.2 \pm 21.0 ppm
Zn			<2000 ppm	91.8 \pm 26.3 ppm
As, Se, Br			<800 ppm	0.3 to 0.4 ppm (As, Se)
Sr, Y, Zr, Nb, Mo			<1000 ppm	0.7 to 125 ppm
Pb			<3000 ppm	0.52 \pm 0.29 ppm
Totals	96.1	96.3	94.4	
Estimates of other phases				
Fe ³⁺ /FeTotal				0.14 \pm 0.01
Na ₂ O	2.0 \pm 0.5 ^a	2.4 \pm 0.4 ^a	2.0 ^b	2.61 \pm 0.35
	6.0 ^d	2.4 ^d	2.4 ^d	
P ₂ O ₅				0.15 \pm 0.07
H ₂ O				0.30 \pm 0.18 ppm
CO ₂				194 \pm 85 ppm
F				211 \pm 118 ppm
S				1109 \pm 224 ppm

^aSurkov et al. (1984), equation specified in Volkov et al. (1986). ^bSurkov et al. (1986), equation specified in Barsukov et al. (1982). Venera and Vega oxides are reported with 2 σ uncertainty following Treiman (2007).

^cAverage and standard deviation (2 σ) of all reported values from 3190 samples in Table S2 of Le Voyer et al. (2019). ^dSemprich et al. (2020). ^{*}This value is reported as Fe₂O₃ in Barsukov et al. (1986). [^]Reported S value recast as SO₃.

and Vega 2 site and an alkaline rock (alkali basalt or leucite) at the Venera 13 site (Treiman 2007). Felsic compositions are also considered for Venera 8 and 13 by Nikolaeva (1990, 1995, 1997) by comparison to terrestrial arc rocks.

3.1.1 Constraints on Primary Mineralogy

Mineralogy was not directly measured by these landers, but the geochemical data has been used to infer mineralogy using multiple approaches: normative calculations, comparing with terrestrial analogs and experimental results, and modeling calculations using the MELTS software package (Ghiorso and Sack 1995; Asimow and Ghiorso 1998).

The major element abundances provided by XRF instruments on Venera 13, 14 and Vega 2 allow the calculation of normative mineralogy, and thus a rock classification, assuming that

Table 3 CIPW normative compositions for compositions in Table 2 and other terrestrial planet basalts. Norms are calculated on a volatile-free basis and renormalized to 100% using <https://minetoshsoft.com/cipw/index.html>. Venus norms are calculated using the Na_2O , P_2O_5 are from MORB (average composition of 3190 samples in Table S2 of Le Voyer et al. (2019))

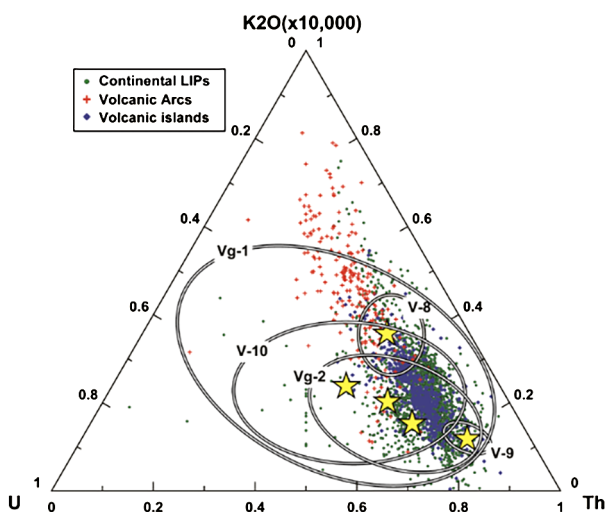
	Ideal Formula	Venera 13	Venera 14	Vega 2	MORB
Quartz	SiO_2	—	—	—	—
Plagioclase		20.1	59.7	58.7	51.6
<i>Anorthite</i>	$\text{CaAl}_2\text{Si}_2\text{O}_8$	20.1	36.4	33.7	28.6
<i>Albite</i>	$\text{NaAlSi}_3\text{O}_8$	—	23.3	25.0	23.0
Orthoclase	KAlSi_3O_8	22.6	1.2	0.7	1.0
Nepheline	$(\text{Na,K})\text{AlSiO}_4$	12.3	—	—	—
Leucite	KAlSi_2O_6	1.3	—	—	—
Diopside	$\text{CaMgSi}_2\text{O}_6$	12.2	11.3	4.1	23.1
Hypersthene	$(\text{Mg,Fe})\text{SiO}_3$	—	12.3	12.3	13.1
Olivine	$(\text{Mg,Fe})_2\text{SiO}_4$	27.9	12.7	23.5	8.1
Ilmenite	FeTiO_3	3.1	2.4	0.4	2.8
Apatite	$\text{Ca}_5(\text{PO}_4)_3(\text{Cl,F,OH})$	0.4	0.4	0.4	0.4

these rocks are unweathered, volatile-free and igneous (Table 3). The Cross, Iddings, Pirs-son, Washington (CIPW) norm calculation (Cross et al. 1902) nominally includes oxides, particularly Na_2O , that was not measured by the XRF on Venus. To perform the norm calculation, Na_2O has been estimated using different methodologies. For Venera 13 and 14, Na_2O content is calculated from the “adopted relation” $[\text{K}_2\text{O}/(\text{K}_2\text{O} + \text{Na}_2\text{O}) \text{ vs. } \Sigma\text{FeO}/(\Sigma\text{FeO} + \text{MgO})]$ (Volkov et al. 1986), presumably derived from analysis of 4 Siberian alkali rock types listed in Table 1 of (Barsukov et al. 1982). For Vega 2, Barsukov et al. (1986) plotted the compositions of ~ 50 terrestrial and lunar gabbroic rocks on an “A-S” diagram, where $A = \text{Al}_2\text{O}_3 + \text{CaO} + \text{Na}_2\text{O} + \text{K}_2\text{O}$ and $S = \text{SiO}_2 - (\text{FeO} + \text{MgO} + \text{MnO} + \text{TiO}_2)$, and derived an estimate for the Vega 2 Na_2O content by comparison. Both methods yield values that are similar to Na_2O contents in MORB (Table 2). The measured XRF values and calculated Na_2O were entered into a volatile-free CIPW norm calculation by Barsukov et al. (1982) and Barsukov et al. (1986) (Table 3). Semprich et al. (2020) used 2.4 wt% and 6.0 wt% Na_2O for Venera 14/Vega 2 and Venera 13, respectively, based on comparison to terrestrial analogue tholeiitic and alkali basalts.

Phosphorous was also not measured by the Venus landers, although it is ubiquitous in igneous materials, generally held in the mineral apatite. Apatite is one of the minerals invoked to explain regions with anomalously lower radar emissivity (see Sect. 3.3). Magmatic phosphorous has also been considered as a source for PH_3 , which may have been detected in the Venus clouds (Greaves et al. 2020; Truong and Lunine 2021).

We have recalculated the normative mineralogy for the Venus lander XRF data including MORB values for Na_2O , P_2O_5 and $\text{Fe}^{3+}/\text{Fe}_{\text{Total}}$ values (Table 2). In agreement with prior normative calculations, Venera 14 and Vega 2 are consistent with olivine-tholeiites, while Venera 13 is consistent with a silica-undersaturated basalt. Apatite is predicted to be a primary phase. Kargel et al. (1993) and Filiberto (2014) compared the analyses with terrestrial analog volcanic rocks and in the case of Filiberto (2014) with experimental crystallization experiments as well. These suggest that Venera 14 and Vega 2 are consistent with terrestrial olivine-tholeiites formed from shallow melting of a potentially hydrous lherzolitic or peridotite source region. Whereas, Venera 13 is consistent with an alkali basalt suggesting

Fig. 3 Ternary plot of U, K, Th values for volcanic rocks from different geodynamic settings on Earth. Yellow stars correspond to the mean values of the measurements by the Venera-Vega landers. Ellipses around the stars correspond to the 1σ measurement errors. Modified from Venera-D JSDT (2017)



a deep partial melting of a potentially carbonated source region. These inferences are also consistent with MELTS modeling where hydrous fractional crystallization is likely needed to produce evolved high alkali rocks (Shellnutt 2013).

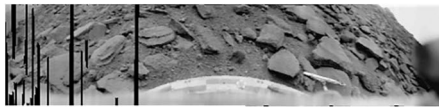
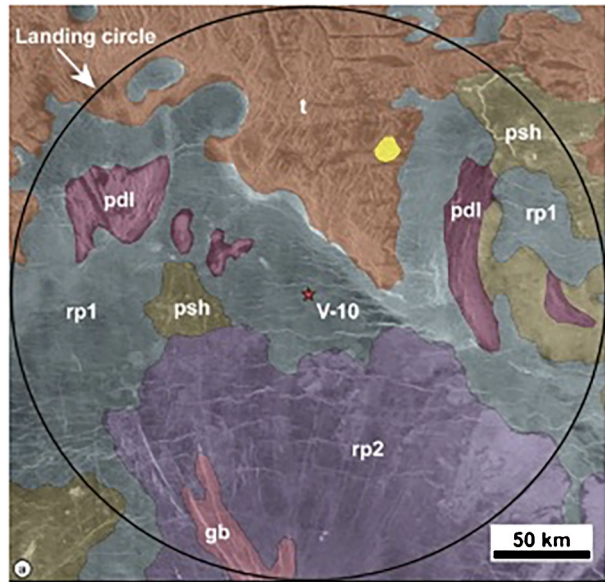
Two important factors limit the value of the Venera/Vega data and prevent their robust interpretation. The most important limitation of the Venera/Vega geochemical data is the low precision and unknown accuracy of the measurements (Tables 1, 2) discussed extensively by Treiman (2007). For example, the U, K, Th data Venera 8 and Venera 9 landers have the smallest errors and show that these rocks are geochemically distinct from one another, and correlate with terrestrial rock types, however the error bars of the Vega 1, 2 and Venera 10 measurements are so large they are almost completely unconstrained (Fig. 3).

Secondly, the Venera and Vega landers followed ballistic trajectories, landing within a ~ 300 km circle within error (Akim and Stepanyantz 1993). Subsequent mapping of the surface using Magellan shows that each landing site included multiple geomorphologic units (e.g., Basilevsky et al. 1992; Weitz and Basilevsky 1993; Basilevsky et al. 2007). For example, the landing circle of Venera 10 includes six various and extensive units Fig. 4). The Venera-10 panorama (Fig. 5, bottom) and inclinometer data indicate that the station is on a flat, sub-horizontal surface. This type of surface is most consistent with the volcanic plains (e.g., the shield plains, psh, and regional plains, rp_1 , rp_2) as the hosting units for the lander and disfavors more structurally deformed units such as tessera terrain (t), densely lineated plains (pdl), and groove belts (gb), although no units within the landing circle can be ruled out.

Thus, in the Venera 10 landing circle and in all other landing sites as well, association of the chemical data with the specific terrains can be made on a probabilistic basis only (Abdrakhimov 2005), which limits the ability to use the morphologic data for geochemical context.

All of the above interpretations are based on the assumption that the chemical weathering did not significantly change the surface material on Venus. Such an assumption is potentially consistent with the lack of free water on the surface, but cannot be reasonably constrained by the available chemical data, particularly because of the large error bars for the sulfur measurements (Table 2). All thermodynamic calculations predict that rocks on the Venus surface

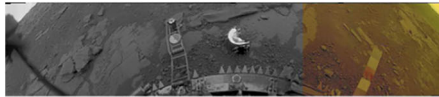
Fig. 4 a) Geological map of the Venera 10 (red star) landing area. Units: t - tessera, pdl - densely lineated plains, gb - groove belts, psh - shield plains, rp1 - regional plains, lower unit, rp2 - regional plains, upper unit. North is up. Modified from Basilevsky et al. (2007)



Venera 9



Venera 10



Venera 13



Venera 14

Fig. 5 Images of the Venus surface recorded by Venera Landers (reprocessed images © Don P Mitchell, used with permission)

will be weathered by the present-day atmosphere (see Sect. 4.1.2). The current observations of secondary mineralogy are discussed in the next section.

3.1.2 Constraints on Secondary Mineralogy

The Venera 9 and 10 landers each carried photometers that measured upward and downward radiation in 5 channels with effective wavelengths centered at 0.54, 0.59, 0.67, 0.77 and 0.87 μm (Economov et al. 1980; Golovin et al. 1983). The surface albedo derived from both sites was <0.2 , consistent with basalts. The Venera 13 and 14 landers each carried two scanning cameras with filters in the blue, green and red. Pieters et al. (1986) used the green and red channels from Venera 13 to produce a “white light” image and show that the rocks at this site are similarly dark in the visible. The data from Venera 9 and 10 show an increase

in reflectance at wavelengths $> 0.7 \mu\text{m}$, which are similar in shape to the charge transfer and crystal field absorptions of ferric oxides (e.g., Morris et al. 1985). Pieters et al. (1986) show that the shape of the curves is consistent with high temperature reflectance spectra of hematite (Fe_2O_3). This result, the low albedo and measured chemistry at these sites are all consistent with the presence of basalts chemically weathered under oxidizing conditions to produce hematite.

There are several lines of observational evidence that the surface of Venus is physically weathered. The photometers on Venera 9 and 10 both recorded a transient dimming of upwelling and downwelling radiation, interpreted to be due to dust liberated by the lander (Ekonomov et al. 1980). Dust was also deposited on the Venera 13 lander ring (Florensky et al. 1983a) and observed to change appearance in consecutive images, indicating active particle transport by wind during the 85 min surface lifetime (Selivanov et al. 1982).

Regolith is present in each of the Venera panoramas surrounding rocks that have varying degrees of layering, fracturing, rounding, pits, and rock burial (Fig. 5), all consistent with physical degradation of the surface rocks (Florensky et al. 1977a,b, 1983b; Garvin et al. 1984; Basilevsky et al. 1985).

The overall strength of the materials was measured by several methods. Venera 13 and 14 carried a penetrometer instrument that measured the load carrying capacity of the surface. The sediment at the Venera 13 site is 1.3 to 5 MPa, similar to a dense sand or weak rock. Unconfined compressive strengths (UCS) of 31 to 126 MPa at the Venera 14 site are less than half that of basaltic rocks. Such a scenario is consistent with the actual densities ($\sim 1.5 \text{ g cm}^{-3}$) and porosities ($\sim 50\%$) inferred from mechanical data recorded by the Venera 13 and 14 probes (Florensky et al. 1983b). Strength was also measured by comparing the dynamics of the impact of the probe with the surface to experiments of a Venera model with various materials on Earth (Basilevsky et al. 1985). The bearing strength of Venera 13 is consistent with materials similar to cemented clastic rocks (Table 4).

Although no images were obtained from the Vega 2 site, load carrying capacities measured from the penetrometer and dynamic loads during lander impact (Marov and Grinspoon 1998; Surkov et al. 1984) allow for an estimation of UCS. Vega 2 recorded a lower porosity ($\sim 20\%$) and higher density ($\sim 2.6 \text{ g cm}^{-3}$) than the Venera landers, but the low UCS ($\sim 10 \text{ MPa}$) and high sulphate content implies a fully weathered and cemented clastic rock, rather than a fresh basalt.

The samples collected by the landers for geochemistry were derived from the uppermost surface. Moroz (1983) states the drill cores were $\sim 1 \text{ cm}^3$ in volume collected from 3 cm depth for both Venera 13 and 14. Barsukov et al. (1986) report a time of 172 sec to acquire and deliver the sample for analysis during Vega 1 and 2. These data both suggest that the samples measured for chemistry by V13, V14 and Vega 2 were from the low-density surface materials and therefore weathered to some degree.

This is corroborated by the abundance of SO_3 in V13, 14 and Vega 2, each of which is elevated above an estimated average MORB composition (Table 4). The source of this SO_3 is most likely due to thermodynamically favored surface - atmosphere interactions which predict atmospheric SO_2 will react with Ca in silicates to produce anhydrite (CaSO_4 ; Zolotov 2007 and references therein). Fegley (2003) calculates if all measured SO_3 in Venera 13, 14, and Vega 2 is contained in anhydrite then that yields $2.8 \pm 1.7 \text{ mass } \%$, $1.5 \pm 1.3 \text{ mass } \%$, $8.2 \pm 2.6 \text{ mass } \%$, for the three landers respectively. Zolotov (2007) points that the S:Ca composition of Venus' rocks indicates incomplete sulfurization of Ca silicates to anhydrite. Dyar et al. (2021) point out that the reported values for S (0.35-1.9 wt%) when considered in light of basalt breakdown reactions modeled by Treiman and Schwenzer (2009) suggest that chemical weathering reactions have gone only 29% to completion at the Vega 2 site,

Table 4 Bearing capacity measurements and inferred surface density and porosity from Venera and Vega landers

Lander	Bearing capacity kg/cm ²	Unconfined compressive strength (MPa)	Inferred density (g/cm ³)	Inferred porosity ^d	Ref	SO ₃ ^{a,f}
V9	40–300 ^a	4–27			b,d	
V10	40–300 ^a	4–27	1.5 or 2.88 ± 0.1 ^c (top 5–7 cm)	1–7%	d c,d	
V13	2.6–10 ^l 4.0–5.0 ^b	0.2–0.9 0.4	1.4–1.5	50–53%	a	1.62 ± 1.0
V14	~2.0 (top 5–10 cm) 4–5 (below 5–10 cm) ^a 65–250 ^{b*}	0.2 0.4 6–22	1.15–1.2 1.4–1.5	60–62% 50–53%	a,b b	0.88 ± 0.77
Vega-2	115	10 MPa	2.6	13%	e	4.7 ± 1.5

Measurement Method: ^aImpact Dynamic Loading, assumes entire lander torus is in contact with the ground
^bPenetrometer/Trellis Girder, ^cGamma Densimeter, ^dRelative to basalt with a density of 3.0 g/cm³ T
^{*}Landed on Lens Cap. [a] Surkov et al. (1984), [b] Basilevsky et al. (1985), [c] Surkov et al. (1977),
[d] Basilevsky et al. (2004) and references therein [e] Marov and Grinspoon (1998) and references therein
[f] Surkov et al. (1986).

and 5–10% at Venera 14 and 13, respectively. However, Vega 2 also has a low analysis total, suggesting either missing elements or substantially more alteration than rocks at Venera 14 and 13. The lower SO₃ amounts measured at Venera 14 relative to the Venera 13 suggest that they are less altered with respect to S consumption. This is consistent with reduced physical weathering relative to Venera 13 rocks (Garvin et al. 1984; Basilevsky et al. 1985), and suggests younger rocks at the Venera 14 landing site.

Thus, the presence of regolith, the relatively low density, the VNIR spectra and the elevated S at the Venera and Vega sites, where measured, are consistent with a weathered basaltic clastic rock that contains hematite and sulfate.

3.2 Near Infrared Imaging

Surface emissivity was derived from the data of several instruments observing the night-side of Venus near 1 μm, using various models. Most of these derivations involved the statistical removal of the correlation with topography, blurred to match the theoretical NIR resolution of 90 to 100 km (Hashimoto and Imamura 2001; Basilevsky et al. 2012). Thus, even if these emissivity derivations may show large differences in average value or amplitude, they are qualitatively comparable, i.e., it can be determined whether a location is high or low emissivity relative to the average. In the following we provide an overview of locations with significant emissivity anomalies.

3.2.1 Low Emissivity Anomalies

Hashimoto et al. (2008) interpret one flyby image of the Galileo Near Infrared Imaging Spectrometer (NIMS) at 1.18 μm wavelength and report that highlands 2 km above mean

planetary radius have on average lower emissivity than other locations. The highlands imaged by NIMS are parts of Ishtar and Aphrodite Terra. A more detailed analysis was not possible due to the high noise of the single image. In this study there was no statistical removal of emissivity correlations with topography, the authors argue that this trend cannot be due to a temperature lapse rate different from their model assumption since this would be a dynamically unstable atmospheric stratification. Such an apparently unstable lapse rate was actually observed by Vega 2, although its cause is not yet clear (Seiff 1987; Lebonnois and Schubert 2017). It is unclear whether there are any significant emissivity anomalies in this data after statistical removal of the trend with topography.

VIRTIS was mostly interpreted with some removal of correlation of topography (Helbert et al. 2008; Mueller et al. 2008; Stofan et al. 2016; Kappel et al. 2016; Mueller et al. 2020). Tessera terrain mostly appears to have lower emissivity compared to plains in the same elevation range. Some of this may be attributed to biased errors in the altimetry (artificial pits from off-nadir reflections) that may be more frequent in tessera terrain due its high roughness (Mueller et al. 2008), however Gilmore et al. (2015) show that roughness does not control the observed emissivity variation within the Alpha Regio tesserae, and that the emissivity is instead correlated to differences in precursor material inferred during earlier mapping (Gilmore and Head 2000). The large tessera plateaus observed by VIRTIS repeat imaging are Alpha Regio, Cocomama Tessera, parts of Thetis Regio, Chimon-mana Tessera, Phoebe Regio, and Dolya Tessera. All are associated with some locally low emissivity, although the latter four are only observed by few VIRTIS images and at unfavorable viewing angles so that the uncertainty is large (Mueller et al. 2008). Chimon-mana Tessera was also observed to have relatively low emissivity by the Venus Monitoring Camera (VMC) (Basilevsky et al. 2012).

There are also volcanic features associated with low emissivity in near infrared data. Basilevsky et al. (2012) find that the central part of Tuulikki Mons, which features a steep sided dome at the summit, has relatively low emissivity in VMC data. Stofan et al. (2016) investigated the emissivity of Themis Regio using a statistical removal of the trend with topography that did not include tessera terrain and find several low emissivity anomalies associated with Mielikki Mons, Shiwanokia Corona and Ukemochi Corona, as well as some patches of regional plains. Kappel et al. (2016) also derived the emissivity of Themis Regio, using the more sophisticated multi-spectrum retrieval method (Kappel et al. 2015) and also found low emissivity in the central plateau of Shiwanokia Corona.

The rock emissivity near 1 μm is dominated by Fe bearing minerals (Hashimoto and Sugita 2003; Dyar et al. 2020, 2021; Helbert et al. 2021). The in situ surface spectra by Venera 9 and 10 are consistent with those of un-weathered basalt samples (Helbert et al. 2021; Filiberto et al. 2020; Cutler et al. 2020; Teffeteller et al. 2022; Zhong et al. 2023) which in turn supports the model of chemical weathering by Dyar et al. (2021) that predicts that emissivity is not strongly affected by alteration because the formation of secondary mineral crusts is self-limiting and cannot completely mask the underlying mineralogy due to their high optical transparency. Therefore, it is likely that the low emissivity locations correspond to a primary rock composition with less Fe-bearing minerals than basalts. There are a number of possible rock compositions that would fit this constraint (e.g., discussions in Gilmore et al. 2015, 2017), but since the tessera terrain constitute a relatively large volume ($\sim 8\%$ of the surface) the discussion has been focused on felsic rocks derived from partial melting of hydrated crust (Hashimoto et al. 2008; Gilmore et al. 2015), as only this process can produce such large volumes of melt from basaltic crust (Shellnutt 2018). This however implies the existence of surface water or a hydrated crust and crustal recycling during the formation of tessera terrain. This was likely not the case for the formation of the volcanic

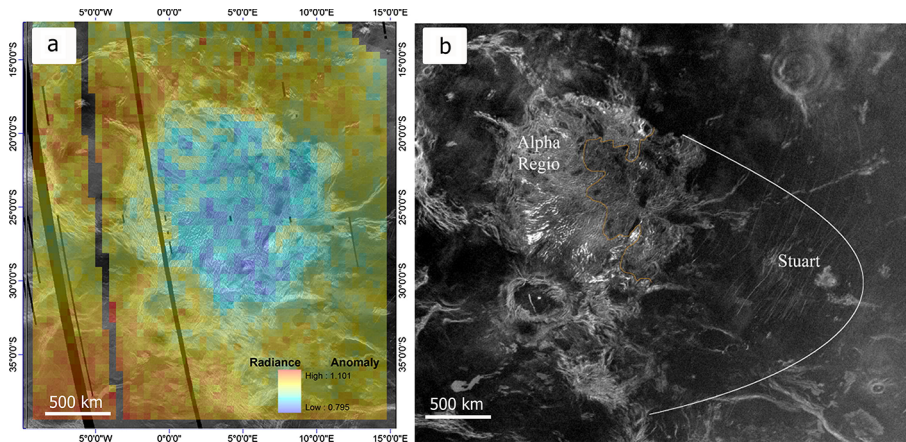


Fig. 6 a) Modified from Gilmore et al. (2015) showing VIRTIS top of atmosphere radiance relative to average radiance versus topography trend, interpreted as low emissivity of Alpha Regio tessera terrain, superposed over Magellan radar image mosaic (2200 m/pixel). b) Modified from Campbell et al. (2015) showing Arecibo circular polarized radar backscatter interpreted as evidence for ejecta from crater Stuart on Alpha Regio

features with low emissivity, however smaller amounts of rhyolite/granite can be produced by anhydrous fractional crystallization of basalt (e.g., Shellnutt 2018).

The presence of particles of micron scale size can also result in lower emissivity. The presence of particles on Venus, in general, can be inferred from the paraboloid impact ejecta blankets (e.g., Campbell et al. 1992), features interpreted as resulting from explosive volcanism (Campbell et al. 2017) and aeolian features (e.g., Greeley et al. 1992). Gilmore et al. (2015) discuss the possibility that the rough tessera terrain collects dust in the topographic lows sheltered from wind. Gilmore et al. (2015) argue that the differences of emissivity within Alpha Regio tessera terrain of comparable roughness is inconsistent with this hypothesis. However, it is also possible that the dust accumulates slowly and that these emissivity differences reflect different ages. The western part of Alpha that does not show low emissivity is one of the few locations where tessera may post-date the plains (Gilmore and Head 2000).

There is however evidence for more recent material on Alpha Regio. Arecibo 12 cm wavelength polarimetric radar observations are interpreted by Campbell et al. (2015) to show ejecta from crater Stuart extending over at least the eastern part of Alpha Regio, however there is no correlation between this same-sense-circular polarized backscatter and the NIR emissivity (Fig. 6). Campbell et al. (2015) estimate the reduction in roughness inferred from the lower radar backscatter to be the equivalent of about 4–7 cm of mantling material. The timescale of settling out of the atmosphere is a function of particle size (Campbell et al. 1992). The presence of ejecta visible in radar data of eastern Alpha Regio therefore strongly suggests some material over the rest of Alpha Regio, with a gradient in particle size decreasing from east to west. It is therefore unlikely that the low NIR emissivity is due to small ejecta particles, since the emissivity is neither correlated with the amount nor with the particle size of ejecta material. The reduction in emissivity must be caused by outcrops that are relatively free of the Stuart ejecta material originating in the presumably basaltic plains, likely by removal of fines by wind.

3.2.2 High Emissivity Anomalies

Locally high emissivity anomalies were reported in several studies of Venus Express VIRTIS data (Helbert et al. 2008; Mueller et al. 2008; Smrekar et al. 2010; Stofan et al. 2016; Kappel et al. 2016; Mueller et al. 2020). The following locations with relatively high emissivity in VIRTIS data coincide with stratigraphically young lava flows: Idunn Mons in Imdr Regio (Smrekar et al. 2010) with recent flows at the summit and on the eastern flank (D’Incecco et al. 2017, 2021; López et al. 2022); Abeona, Chloris, Mertsegger, and Mielikki Montes in Themis Regio (Smrekar et al. 2010; Stofan et al. 2016); Innini and Hathor Montes in Dione Regio (Smrekar et al. 2010), as well as Semiramus, Zywie, Latta, Shulamite, Ukemochi, Shiwankia Corona, Nzambi, Bibi Patma Coronae in Themis Regio (Stofan et al. 2016). Additionally, there is an area of significantly increased emissivity coinciding with the radar bright inner paraboloid ejecta feature associated with crater Sabin in Themis Regio (Mueller et al. 2020).

As discussed in Dyar et al. (2020), the observed local increase of emissivity is 0.02 to 0.06 according to the most recent radiative transfer models (Kappel et al. 2016; Mueller et al. 2020). This emissivity difference is consistent with the chemical weathering of basalt under Venus surface conditions, where Fe^{2+} in silicates is converted to Fe^{3+} in oxides with higher $\sim 1 \mu\text{m}$ emissivity (e.g., Dyar et al. 2020; Filiberto et al. 2020; Cutler et al. 2020; Tefetteller et al. 2022; Zhong et al. 2023). The high emissivity values and their correspondence with young flows has led to the interpretation that these regions are locations of unweathered and thus recent basaltic volcanism relative to the average plains (Smrekar et al. 2010; Stofan et al. 2016; D’Incecco et al. 2017, 2021; López et al. 2022). Smrekar et al. (2010) estimated the timing of this volcanism to be $< 250,000$ years, based on calculated rates of resurfacing for Venus, however laboratory studies of olivine ($\text{Fe, Mg})_2\text{SiO}_4$ at Venus temperatures imply much faster rates of oxidation on the order of days to months (Filiberto et al. 2020) or 10s–100s years (Zhong et al. 2023).

These observations highlight the urgent need for both laboratory studies of the weathering of rocks and minerals under Venus conditions and laboratory measurement of their $1 \mu\text{m}$ emissivity. For example, the NIR emissivity of natural basalts can vary by ~ 0.07 due to FeO content (Helbert et al. 2021), thus emissivity variations must consider variability in the initial composition of the lavas. Emissivity is also dependent on the type, distribution and thickness of secondary minerals. Both thermodynamic calculation and laboratory experiments predict the formation of other secondary minerals such as anhydrite, which is predicted to have a low emissivity. Modeling of the diffuse reflectance and derive emissivity of two-component mixtures of mineral particulates predict that the 10–20% hematite shifts the emissivity signature of basalt by 0.01–0.03 units and 20% anhydrite shifts the emissivity of basalt by 0.04–0.06 unit (Dyar et al. 2021). The effects of grain size in $1 \mu\text{m}$ emissivity are unclear; limited measurements ($n = 4$) show that particle size is not a dominant factor (Helbert et al. 2021). Much work remains to be done.

3.3 Magellan

3.3.1 Global Survey of Venus Highlands

Pioneer Venus and Magellan data show that many of Venus’ highlands have distinctly elevated values of radar reflectivity relative to the global average (Masursky et al. 1980; Ford and Pettengill 1983) and thus low values of radar emissivity at their summits (Pettengill et al. 1992). The reflectivity values are ascribed to the presence of minerals or compounds

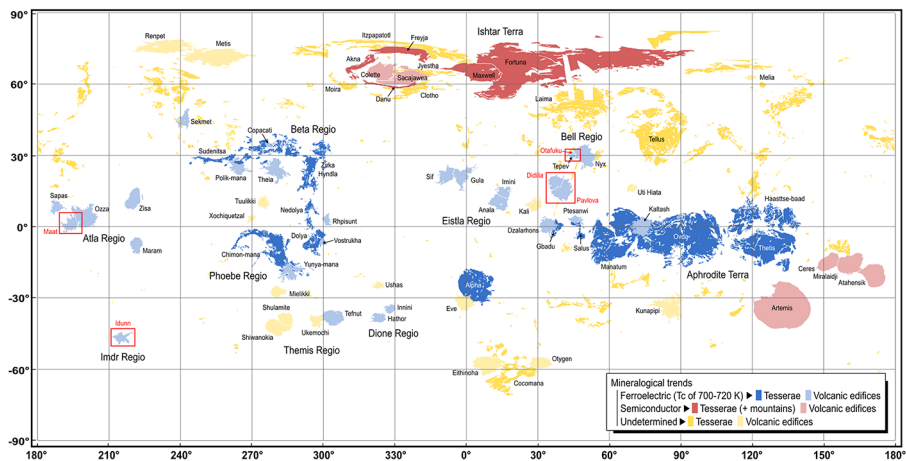


Fig. 7 Mineralogical trends on volcanic edifices (Brossier et al. 2020) and tesserae and mountain belts (Brossier and Gilmore 2021). Red frames indicate sites of possible recent activity (Fig. 8)

with a high dielectric constant as inclusion or coatings on surface rocks, as materials with high dielectric constants will enhance their radar reflectivity and lower their radar emissivity (Pettengill et al. 1992; Campbell 1994). Proposed minerals include: (1) pyrite (Pettengill et al. 1988; Klose et al. 1992; Wood and Brett 1997; Kohler 2016; Port et al. 2016; Berger et al. 2019; Sempich et al. 2020), (2) metallic frosts like lead and bismuth sulfides (Brackett et al. 1995; Pettengill et al. 1996; Schaefer and Fegley 2004; Kohler et al. 2015; Port et al. 2020), and (3) ferroelectric minerals, such as chlorapatite or perovskites that become highly dielectric at certain temperatures (Curie temperatures; Arvidson et al. 1994; Shepard et al. 1994; Treiman et al. 2016). These type and volume of dielectric materials are a function of rock composition, atmospheric composition, temperature and, if due to surface – atmosphere reactions, the length of exposure time at the surface. Because of the temperature dependence of these reactions, the detailed description of the variations in radar emissivity with altitude provide new insights into the relative composition and potential exposure age of the surface materials.

Klose et al. (1992) compared a sample of major volcanoes, mountains and tesserae and recognized differences in the style, magnitude and altitude of emissivity variations between and among these regions. Treiman et al. (2016) also noted similar differences in the radar emissivity signatures between Ovda Regio tessera and Ishtar Terra. More recently, Brossier et al. (2020) and Brossier and Gilmore (2021) measured and compared the variation of radar emissivity with altitude (and thus temperature) to understand the variety of radar emissivity signatures among all major venusian highlands. All of these studies conclude that variations in radar emissivity indicate differences in the composition, volume and type of dielectric materials in these regions.

As shown in Fig. 7, the majority of volcanoes and coronae on Venus (e.g., Maat and Ozza Mons; Brossier et al. 2020) and most tesserae (Aphrodite Terra, Alpha, Beta, and Phoebe regions; Brossier and Gilmore 2021) are compatible with the presence of ferroelectrics. The elevation and shape of the emissivity patterns indicate the presence of at least two ferroelectric compounds with distinct Curie temperatures, varying from 700 K to 720 K (6054–6056 km). This varying “critical altitude” reported in Klose et al. (1992) and seen by Brossier and colleagues could be due to different primary mineralogy, or local differences

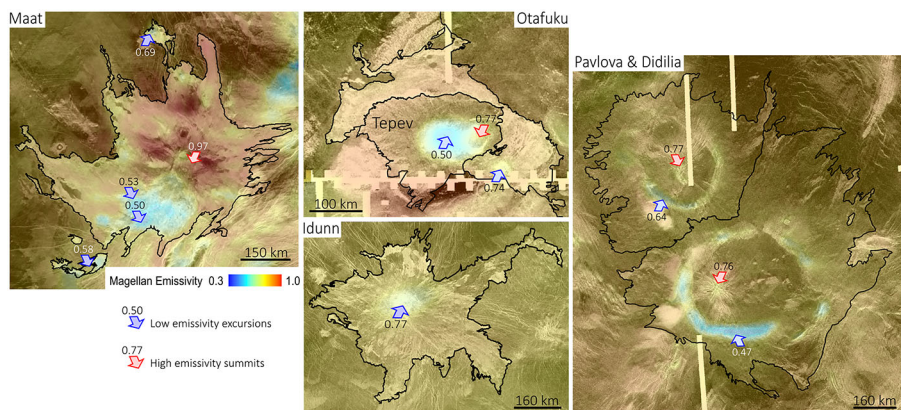


Fig. 8 Radar emissivity maps overlapping SAR images of Maat (194°E, 1°N), Otafuku (45°E, 30°N) and Idunn montes (215°E, 47°S), as well as Pavlova and Didilia coronae (40°E, 16°N). The high radar emissivity values found at their summits suggest the presence of young, unweathered lava flows

in the atmospheric composition or temperature at the time of the formation of the minerals by weathering (Treiman et al. 2016; Strezoski and Treiman 2022). The wide distribution of ferroelectrics shows that these minerals are common to volcanic, tesserae and mountain materials.

Conversely, the emissivity pattern of volcanoes, tesserae and mountain belts in western Ishtar Terra and the coronae in eastern Aphrodite Terra (Diana – Dali chasmata) are more consistent with the presence of semiconductor materials rather than ferroelectrics (Treiman et al. 2016; Brossier et al. 2020; Brossier and Gilmore 2021; Strezoski and Treiman 2022). The different signatures observed on Venus' highlands could be associated with mineralogical variability, perhaps related to differences in geologic settings (mantle processes), or surface temperature gradient.

Additionally, Brossier et al. (2020) reported that emissivity signatures of Maat, Idunn and Otafuku montes and the novae within Pavlova and Didilia coronae are consistent with lower volumes of ferroelectric minerals, consistent with relatively recent and less weathered lava flows (Fig. 8). These volcanic edifices are associated with presumably active hotspots that are among the most likely sites for recent or current volcanic activity on Venus based on geophysical (Smrekar 1994; Stofan et al. 1995) and morphological (Herrick and Hensley 2023) data. A less weathered surface has also been suggested for Idunn based on 1- μ m VIRTIS data (Smrekar et al. 2010) (see Sect. 3.2). Thus, the radar emissivity data provide an independent constraint on recent volcanic activity on Venus in agreement with both 1- μ m emissivity and gravity signatures.

3.3.2 Local Investigations in Atla Regio

The two largest volcanoes on Venus, Maat and Ozza Montes, display multiple reductions in radar emissivity at different altitudes including, atypically, values at or close to mean planetary radius (MPR = 6051.8 km) (Fig. 9; e.g., Wilt 1992; Robinson and Wood 1993; Brossier et al. 2020). The range of Curie temperatures are derived from the altitude and magnitude of the emissivity excursions, corresponding to values of 693–731 K over a range of elevation of 6052.5 km to 6056.7 km. Low elevation excursions at Maat and Ozza indicate ferroelectric minerals at higher Curie temperatures than any excursions previously observed

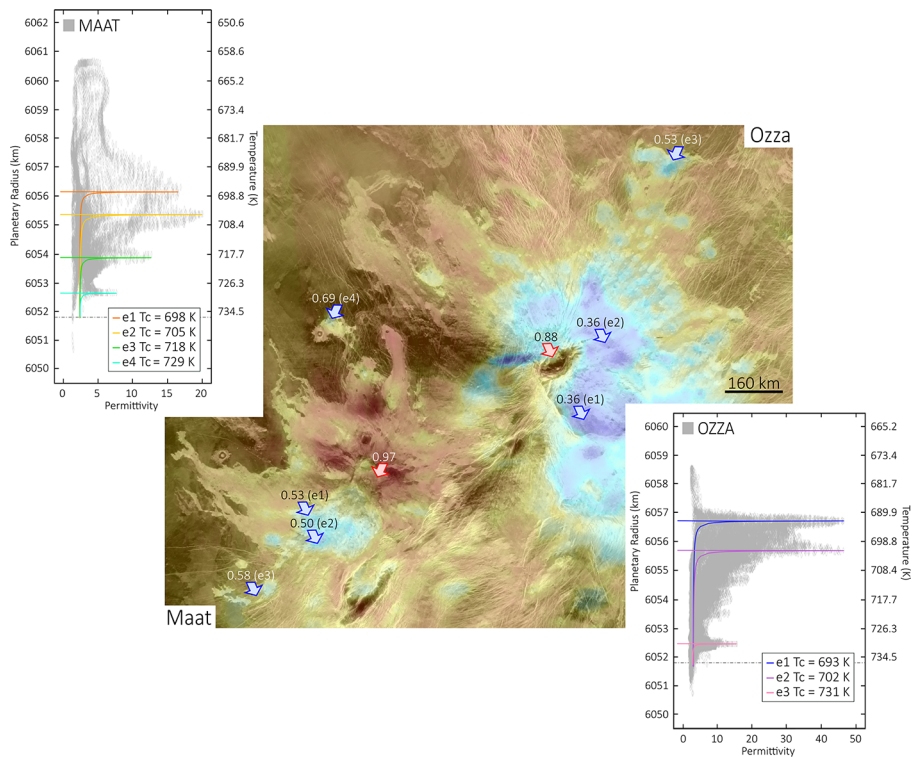


Fig. 9 Radar emissivity map overlapping a SAR image of Maat and Ozza montes located in Atla Regio (198°E, 4°N). Elevation – permittivity plots showing the multiple excursions detected on the two volcanoes (Brossier et al. 2021). Here, permittivity values are derived from radar emissivity values (Campbell 1995), while temperatures are given by the Vega 2 lander data (Seiff 1987; Lorenz et al. 2018). Application of the ferroelectric model (Shepard et al. 1994) to reproduce the low emissivity excursions (color-coded curves)

on Venus. Brossier et al. (2021) showed that specific ferroelectric signatures correlate with individual lava flows, indicating that the ferroelectric minerals are related to rock chemistry as opposed to the regional deposition of atmospheric precipitates.

Laboratory measurements of the Curie temperatures of minerals at Venus temperatures and radar wavelengths are necessary to constrain the candidate minerals to explain the emissivity patterns on Venus observed by Magellan, VERITAS and EnVision. Table 5 contains the list of ferroelectric minerals measure at Venus temperature found in the current literature. From this non-exhaustive list, the derived Curie temperatures from Magellan emissivity are consistent with the mineral chlorapatite ($\text{Ca}_5(\text{PO}_4)_3\text{Cl}$) and perovskite oxides (e.g., $\text{X}_2 + \text{TiO}_3$) and inconsistent with other substances, including GeTe which has been previously proposed for Venus. Using the method of Shepard et al. 1994, Brossier et al. (2021) calculated minimum estimates for the volumes and types of ferroelectric inclusions responsible for each emissivity excursion and they obtained volumes in the ppm range (6–113 ppm). Experiments on the formation, stability, and Curie temperatures of candidate ferroelectrics at Venus conditions will advance our understanding of the petrology of these volcanoes and the nature of the surface – atmosphere interactions.

Brossier et al. (2022) recently extended their investigation in Ganis Chasma, a rift valley in Atla Regio where recent activity was already suggested based on the superposition of rift

Table 5 List of ferroelectric minerals with Curie temperatures near Venus surface temperature (Brossier et al. 2021). Minerals proposed specifically for Venus are indicated by an asterisk (*). References: (1) Subbarao 1973; (2) Treiman et al. 2016; (3) Brackett et al. 1995; (4) Kadlec et al. 2011; (5) Shepard et al. 1994; (6) Young and Frederikse 1973

Compound	Formula	Curie Temp. T _c (K)	Curie Constant	Refs
Barium Bismuth Tungstate	Ba(Bi _{0.7} W _{0.3})O ₃	723		1
Cadmium Iron Niobate	Cd(Fe _{0.5} Nb _{0.5})O ₃	723		1
Cadmium Scandium Niobate	Cd(Sc _{0.5} Nb _{0.5})O ₃	703		1
Chlorapatite*	Ca ₅ (PO ₄) ₃ Cl	675–775		2
Lead Bismuth Tantalate	PbBi ₂ Ta ₂ O ₉	703		1
Germanium Telluride*	GeTe	623–670	~ 1.0 × 10 ⁵	1,3,4
Lead Bismuth Tantalate – Niobate*	Pb ₂ Bi(Ta,Nb)O ₆	693–748		1,5
Lead Tantalate – Niobate*	Pb(Ta,Nb) ₂ O ₆	533–843		5,6
Lead Titanate*	(Pb(Ba,Sr,Ca))TiO ₃	110–763	1.1 × 10 ⁵	1,5,6
Sodium Niobate-Tantalate*	Na(Nb,Ta)O ₃	627–753		1,5
Lutetium Chromite	LuCrO ₃	713		1
Potassium Lithium Niobate	K ₃ Li ₂ Nb ₅ O ₁₅	703		1
Potassium Niobate – Tantalate*	K(Nb,Ta)O ₃	2–708	2.4 × 10 ⁵	1,5,6
Strontium Bismuth Niobate	SrBi ₂ Nb ₂ O ₉	713		1

structures on young impact deposits (Basilevsky 1993). Ganis Chasma bears several sites with high (1-μm) emission with varying intensity over several days or months (Shalygin et al. 2015). Shalygin and colleagues suggested that these transient high emission sites are possibly associated with short-lived effusive activity, locally causing significant increases of surface temperatures. According to Brossier et al. (2022), the pattern of radar emissivity in these sites indicates the presence of ferroelectrics with subtle differences in the mineral composition, in agreement with the other volcanoes in Atla Regio (Brossier et al. 2020, 2021). They also demonstrated that these sites are consistent with relatively young and unweathered materials, providing independent corroboration of active (rift-associated) volcanism in Ganis Chasma since the 1990's.

3.4 Morphology

The rheology of lava is affected by its composition (e.g., Giordano et al. 2008), therefore the morphology of volcanic features can - in some cases - give evidence of lava composition. Generally, the amount of SiO₂ increases lava viscosity due to the formation of polymer chains in the melt (Baker et al. 1992). The interpretation is complicated by the fact that the rheology of silicate lavas is also highly dependent on temperature, volatile content, and shear forces (Lejeune and Richet 1995), all of which are expected to be different on Venus when compared to more accessible morphological analogues with known compositions (Head and Wilson 1986). In addition, it is not clear that the climate of Venus is stable over long durations, such that formation of any volcanic features at different periods of time might have taken place under very different ambient temperature conditions (Bullock and Grinspoon 1996, 2001, Noack et al. 2012), which influence the cooling rate (Snyder 2002) and thus viscosity contrasts within bodies of lava (Stofan et al. 2000). The high atmospheric pressure inhibits exsolution of volatiles (Garvin et al. 1982; Head and Wilson 1986) which is

expected to reduce the viscosity of basalt and rhyolite lavas by 20–30% and an order of magnitude, respectively (Bridges 1997).

Most volcanic features observed by Magellan on Venus are morphologically consistent with basaltic compositions (Head et al. 1992). Features that have been discussed as potentially indicative of non-basaltic composition are steep sided domes (Pavri et al. 1992), festoon flows (Moore et al. 1992), sinuous rilles and canali (Baker et al. 1992; Komatsu et al. 1993).

Steep sided domes are features that are 10 to 10² km diameter, hundreds of m high, typically near circular volcanic features, that resemble pancakes (Pavri et al. 1992). The morphology and thickness to diameter ratio suggests slow emplacement of highly viscous lava, similar to dacite or rhyolite domes on Earth (Pavri et al. 1992; Fink et al. 1993). Stofan et al. (2000) on the other hand propose that lava inflates the flow under a cooled crust that fractures and anneals as it expands. Stofan et al. (2000) find that basalt is a more likely composition in the context of this mechanism since the high viscosity of rhyolite would not allow annealing, which however would not be true under a significantly hotter climate.

Festoon flows have been proposed to be composed of more silicic lavas than basalt for similar reasons as the steep sided dome: the large thickness and relatively broad interior structures suggests a high lava viscosity during emplacements (Head et al. 1992; Moore et al. 1992), and resemble rhyolitic coulees on Earth (Fink and Anderson 1999). Only three of these flows are found on Venus. One of them occurs on tessera terrain in Ovda Regio, which has been mentioned in support of the hypothesis tessera are more silicic than basalt, but recently Wroblewski et al. (2019) find that the morphology of this particular flow is more consistent with basalt.

Sinuous rilles on Venus resemble features of the same name on the Moon: single meandering channels that are widest and deepest near the source and appear to incise into pre-existing terrain (Baker et al. 1992; Komatsu et al. 1993; Oshigami et al. 2009). This suggests thermal erosion by a turbulent low viscosity lava as the formation mechanism, where underlying material is partially melted and not just mechanically eroded (Baker et al. 1992; Komatsu et al. 1993). Basalt lava is formed by partially melting ultramafic mantle material and thus erupts close to its solidus temperature (~1100 °C), which means that its capability to thermally erode underlying basalt is limited (Komatsu et al. 1993; Gregg and Greeley 1993; Fagents and Greeley 2001). Increased ambient temperature increases the substrate's susceptibility to thermal erosion due to the lower amount of heat that needs to be transferred from the lava. Ultramafic magmas formed by higher degrees of partial melting would have lower viscosity – increasing turbulence – and significantly higher eruption temperatures (~1600 °C), thus have a much higher potential for thermal erosion (Komatsu et al. 1993). Turbulent ultramafic komatiite lava flows likely occurred on Earth during the Precambrian (Kilburn 2000; Williams et al. 2001) and high temperature ultramafic eruptions have likely been observed on Io (McEwen et al. 1998), thus there is some support for the hypothesis that mantle temperature higher than that of recent Earth could result in such lava compositions. Komatiite consists mostly of Mg-rich olivine (Williams et al. 2001) and may be more resistant to chemical weathering compared to tholeiitic basalt (see Sect. 4).

Canali type channels (Head et al. 1992; Baker et al. 1992; Komatsu et al. 1993), are very distinct from sinuous rilles and more similar to terrestrial rivers in that they can meander over distances over thousands of km at near constant width and depths (Oshigami and Namiki 2007). They exhibit morphologies suggesting fluvial sediment deposits such as scroll bars, streamlined islands, bird-foot-deltas, and oxbows (Kargel et al. 1994), indicating that some particulate materials were transported and redeposited by a fluid. They also appear to have levees in some locations (Oshigami and Namiki 2007), which is a common feature

of lava channels. Assuming that the channels formed by deposition would require tremendous volumes of lava and resurface large parts of the planet within the cooling timescale of the flow (Komatsu et al. 1993). Thermal erosion by a silicate lava is unlikely since the heat loss would increase the viscosity long before traveling the entire distance (Gregg and Greeley 1993; Williams-Jones et al. 1998). Mechanical erosion by a fluid that remains liquid at ambient or very near to ambient temperatures fits the observed morphology better; proposed compositions are carbonates, sulfates, and elemental sulfur (Gregg and Greeley 1993; Kargel et al. 1994). The question whether the proposed compositions remain liquid at ambient (e.g., Treiman 1994) has to be discussed in the context that there is no reason to assume that the climate is stable and may have been 150 K hotter in the past (Bullock and Grinspoon 1996, 2001; Noack et al. 2012).

4 Laboratory Data

4.1 Thermodynamic and Experimental Constraints on Surface Mineralogy

Laboratory experiments and modeling are powerful tools to constrain the mineralogy of surface with acknowledgment of the limitations and assumptions of each approach. Thermodynamic modeling has been extensively used to predict equilibrium alteration mineralogy of the surface; while, more recently, experimental studies have been employed to investigate mineral stability, as well as the rate of mineral alteration. Thermodynamic modeling can calculate and explore a larger parameter space than experimental approaches due to the speed of modeling, but this approach typically assumes equilibrium conditions. Experiments are limited to laboratory timescales, where the amount of reaction is limited by kinetics. Combining modeling and experimental results can therefore cover a larger range of parameter space, alteration processes, and timescales than either approach alone.

Both of these methods rely on a number of variables such as temperature and pressure, oxygen fugacity, sulfur fugacity, and atmospheric composition. Most of these parameters are not well constrained in the near-surface atmosphere on Venus (e.g., Fegley 2003); approaches to mitigate this uncertainty can include using a range in conditions covering the predicted values for Venus. Thermodynamic calculations can more easily accommodate investigations over ranges in these variables, while it takes numerous, often long, experimental runs to accomplish the same feat in the laboratory. A second assumption is the starting composition (i.e., primary mineralogy or chemistry) of rocks on Venus. Most investigations have used minerals likely to be present on Venus based on our understanding of petrology and planetary evolution (e.g., olivine, pyroxene, plagioclase feldspar), as well as the limited rock chemistries that have been measured (e.g., basalt). However, other Venus-specific materials, suggested based on mission observations, have also been investigated (e.g., apatite and pyrite, as possible candidates for the high radar emissivity anomaly; Treiman et al. 2016; Fegley et al. 1995). Due to the number of variables (and unknown values) involved, few studies have utilized the exact same conditions when examining minerals on Venus, but despite this, some overall trends have been determined, which are discussed below.

4.1.1 Thermodynamic Modeling of Venus Weathering

Several studies have performed thermodynamic calculations to assess the stability of a variety of minerals at the surface of Venus. These studies have used different starting compositions and different environmental conditions, ranging from those of the modern Venus

Fig. 10 General trends in Venus weathering from thermodynamics. See Zolotov (2018) for details

Carbonates	➔	Sulfates
Fe-oxides, sulfides	?	Dependent on f_{O_2} , f_{S_2}
Fe in silicates	?	Dependent on f_{O_2} , f_{S_2}
Ca, Na in silicates	➔	Anhydrite, thenardite
H ₂ O, OH-endmembers	➔	Dehydrate
F-endmember amphibole, Phlogopite, Quartz		Stable

atmosphere, to more water-rich atmospheres that possibly reflect an ancient Venus environment (Semprich et al. 2020). Some studies have focused on specific mineral-gas reactions, while others use more complex modeling that involves reactions between many gases and solids (i.e., Gibbs free energy minimizations). A summary of solid-gas reactions on Venus can be found in Zolotov (2018) and is summarized in Fig. 10. The advantage of thermodynamic modeling over experiments is the ability to easily cover a wide range of parameter space, something that is useful for examining Venus in the current time as we still have poor constraints on the conditions of the near surface environment. This modeling is limited, however, by available databases and their quality, our knowledge of the actual conditions at the surface of Venus, and the fact that thermodynamics determines equilibrium states, which may or may not be achieved on natural planetary surfaces due to rates of reactions.

Gibbs free energy minimization modeling efforts have covered a wide range of conditions, but a broad division can be made between those that included sulfur species as an atmospheric gas species, and those that did not. Two studies that conducted modeling in H₂O-CO₂ atmospheres without sulfur, those of Khodakovskiy et al. (1979) and Semprich et al. (2020), determined a number of hydrous phases (e.g., micas, amphiboles, tremolite) were stable products of basalts, alkali basalts, and granite at conditions of the mean planetary radius. The exact phases differ due to differences in the model parameters, updated databases, and the use of solid solutions in the work of Semprich et al. (2020).

Modeling of reactions of basalts and granites that included sulfur species in the atmosphere resulted in stable plagioclase, orthopyroxene, clinopyroxene, K-feldspar, quartz, and anhydrite at different modeled conditions (Barsukov et al. 1982; Klose et al. 1992; Treiman and Schwenzer 2009; Semprich et al. 2020). Differences due to use of solid solutions in some models but not others, as well as differences in databases and input parameters, can account for some discrepancies in the model outputs. For example Semprich et al. (2020), Treiman and Schwenzer (2009), Klose and Zolotov (1992) find cordierite (Mg,Fe)₂Al₃(AlSi₅O₁₈) to form as a result of reactions of anorthite and diopside at high oxygen fugacities in basalt and alkali basalt compositions, while studies that do not include solid solutions predict andalusite Al₂(SiO₄)O to be a product (e.g., Klose et al. 1992). The stability of iron-bearing oxides and sulfides is highly dependent on the chosen conditions of the model, but multiple studies show pyrite to only be stable at high elevations (Semprich et al. 2020; Klose et al. 1992) (though Barsukov et al. (1982) calculate either magnetite or pyrite to be present at the mean planetary radius), pyrrhotite is shown to only be stable at reduced conditions that are unlikely to be present on Venus (Klose et al. 1992; Semprich et al. 2020), hematite solid solutions with ilmenite (FeTiO₃) and geikielite (MgTiO₃) are stable to lower oxygen fugacities than pure hematite (Zolotov 1994; Semprich et al. 2020). Calcite was not found to be stable at any elevation in the sulfur-bearing models, but Semprich et al. (2020) did show dolomite and calcite to be stable in conditions of low oxygen fugacity and high sulfur fugacity for limited bulk compositional space (i.e., having low f_{SO_2}/f_{S_2}).

Thermodynamic calculations have also been applied to specific open questions for Venus, particularly to explore possible mineralogical causes of the low radar emissivity regions. Calculations by Schaefer and Fegley (2004) and Port and Chevrier (2021) addressed the likelihood and stability of minerals composed of a number of volatile metals (e.g., tellurium, mercury), and found neither elemental Te nor Hg compounds are likely to be responsible for this phenomenon on Venus, as had been proposed previously by Brackett et al. (1995) and Pettengill et al. (1996) due to their high dielectric constants. Treiman et al. (2016) proposed conversion of fluorapatite, the most common variety of apatite in terrestrial igneous systems, to chlorapatite by reaction with HCl in the Venus atmosphere could be a source for a ferroelectric mineral. Other studies have calculated the stability of different iron oxides or sulfides at high elevations (Fegley et al. 1995; Zolotov 2018). However, the stability of these phases is largely dependent on f_{O_2} and f_{S_2} , which are not well constrained, and for this reason, thermodynamic calculations cannot resolve this question without further measurements from missions.

4.1.2 Experiments

Crystallization experiments are used to determine the minerals initially formed by the cooling of lava or magma, and also can provide information about mantle mineralogy if conducted at high pressure. These experiments have not been extensively conducted for Venus because of the lack of chemical data from rock units, and due to the quality of the measurements we do have (e.g., large uncertainty in MgO a key parameter for igneous petrology and a lack of data on Na₂O or P₂O₅, both of which influence mineralogy). However, experimental results from studies on terrestrial compositions have been useful in helping interpret the rocks measured on the surface (e.g., Filiberto 2014).

Weathering experiments to determine stable minerals, reaction products, and reaction rates have been the major focus of current Venus experimental work. Different experimental approaches have been applied to study Venus weathering, including heating in air or CO₂ (typically looking at oxidation or dehydration reactions, e.g., Knafelc et al. 2019; Cutler et al. 2020; Filiberto et al. 2020; Johnson and Fegley 2000, 2002, 2003; Teffeteller et al. 2022), heating with sulfur-bearing gases (e.g., Aveline et al. 2011; Fegley and Prinn 1989; Port and Chevrier 2020; Port et al. 2020; Reid 2021), heating under complex atmospheres (Radoman-Shaw et al. 2022; Santos et al. 2023) and observations of basaltic weathering in the field (McCanta et al. 2014). These studies have been done at ambient pressure or at Venus-relevant pressures. Overall, experimental results have been in agreement with predictions of Venus weathering from thermodynamics, with the exception of reactions that may take place over long timescales, and thus are not observable on experimental timescales. Both experimental and modeling methods suggest that primary minerals on the Venus surface (as well as glasses and bulk rocks) will lose Fe, Ca, and Na to weathering reactions that will produce secondary mineral phases such as Fe-oxides, Fe-sulfides, or sulphates (Ca- or Na-) on their surfaces. This will also result in the formation of more Mg-, Al-, and Si-rich phases such as forsterite, aluminosilicates, and quartz (e.g., Zolotov 2018).

A critical aspect of weathering is the rate at which minerals weather. As noted by Johnson and Fegley (2000, 2002, 2003), even if a mineral is not stable at the current surface conditions of Venus, a slow rate of breakdown may allow it to persist on the surface over geologic time. This may allow minerals formed in past climate eras by different weathering styles to still exist today. Determining reaction rates involves a number of time series experiments, as demonstrated by Fegley and Prinn (1989), who studied the rate of calcite reaction, and Johnson and Fegley (2000, 2002, 2003), who studied the rate of tremolite dehydration.

Calcite reaction was shown to take place faster than tremolite dehydration in these studies, and calcite was observed to react relatively quickly in mineral suites exposed to complex Venus atmospheres in Radoman-Shaw et al. (2022) and Santos et al. (2023). Additionally, mechanisms of reaction are important to determine, as some reactions may produce protective coatings of secondary minerals that limit further reaction progress, leaving only thin layers of surface minerals changed from their primary composition (discussed in King et al. 2018). Thus far, no experimental studies have reported finding reactions limited by a protective surface layer. Both reaction rate and mechanism are critical to determine to understand the mineralogy of the Venus surface today and in the past, and how mineral-gas reactions influence both the surface and atmospheric chemistry over time.

4.2 High Temperature Spectroscopy

4.2.1 Theory

One of the problems with interpreting Venus surface spectra is the need to understand spectral properties of geologic materials at high temperatures, for which little laboratory data exist. High (and low) surface temperatures affect band positions in mineral spectra as predicted by crystal field theory. In the few cases where experimental data exist, temperature (T) and pressure (P) have opposing effects (i.e., shifts to higher and lower wavelengths, respectively) on band positions, but such conclusions are difficult to generalize because they vary with crystal structures and site geometries of different mineral groups. Existing data are a mishmash of emissivity and reflectance measurements taken under various viewing geometries acquired over a period of more than 60 years. There is a need for clarity in understanding the relationships among high- and low-T spectra of single minerals and the underlying physical characteristics that govern them.

Pioneering work from the 1960's to 1980's led to the use of crystal field theory for understanding spectral feature positions, summarized in the seminal book of Roger Burns (1970, 1993), *Mineralogical Applications of Crystal Field Theory*. It details how spin-allowed crystal field transitions take place when transition metal cations reside in different types of ligand fields, splitting the energy levels of *d*-orbital electrons in response to asymmetry induced by the crystal structure. An incident photon may be absorbed at certain wavelengths, exciting an electron from a lower to a higher energy state (Burns 1993). If the resultant electronic transition is spin-allowed, it produces a prominent absorption feature, such as the familiar 1 and 2 μm Fe^{2+} bands in pyroxene (Adams 1974; Cloutis and Gaffey 1991), which result from transitions made possible by splitting within the e_g and t_{2g} orbitals around Fe cations in the M1 and M2 crystallographic sites. The relative intensities of such absorptions increase with the asymmetry of the (in this case, octahedral) site (Burns 1993). The energy of crystal field splitting and the resulting band positions are a function of the ligand field, which changes in response to the structure and composition of the mineral studied.

Crystal field splitting (Δ) describes the difference in energy between the lowest and highest orbital in the electron cloud surrounding (generally) a transition metal cation. The energies of Δ vary according to several factors including (1) the symmetry and coordination number of the polyhedral (often the silica tetrahedron in its various forms), (2) the valence state of the cation, (3) the strength of its bond with the surrounding anions, (4) the distance between the cation and the surrounding anions, (5) pressure, and (6) temperature. Of particular interest are the relative magnitudes of these different variables on spectra, and for Venus, particularly the latter two.

In general, the largest factor affecting Δ values is coordination number. The separation (also termed Δ) between energy levels can be expressed as:

$$\Delta_o : \Delta_c : \Delta_d : \Delta_d = 1 : \frac{8}{9} : \frac{-1}{2} : \frac{-4}{9}.$$

These ratios correspond to the magnitude of the splitting of the d -orbitals between t_{2g} orbitals and e_g orbitals. The Δ values also represent the amount of energy (photon) that will be needed to move an electron from the low energy orbitals to the high energy ones, and thus they correspond to the energies of bands seen in spectra.

The Δ values are also a function of valence state and type of ligand, in the general order of $\text{Mn}^{2+} < \text{Ni}^{2+} < \text{Co}^{2+} < \text{Fe}^{2+} < \text{V}^{2+} < \text{Fe}^{3+} < \text{Cr}^{3+} < \text{V}^{3+} < \text{Co}^{3+} < \text{Mn}^{4+}$. However, coordination number, valence state, and bond strength rarely change with pressure and temperature. On the other hand, bond length is directly related to Δ , and it changes with both pressure (P) and temperature (T).

Pressure effects on Δ are described by the relation (Burns 1993):

$$\frac{\Delta_P}{\Delta_0} = \left(\frac{R_0}{R_P} \right)^5,$$

where Δ_0 and R_0 are the splitting and typical cation to anion distance under ambient conditions and Δ_P and R_P represent those parameters at a specific pressure. However, such changes in bond length can be difficult to generalize because they depend on the compressibility of each coordination polyhedron, which is in turn a function of bond type/strength. High pressure may increase the degree of covalent bonding, increasing peak intensity. When pressure increases do cause contractions of cation-anion bonds, higher Δ and (lower) blue-shifted peak energies relative to ambient conditions are observed. However, it must be noted that such pressure effects have primarily been observed under conditions in the Earth's mantle, where $P \geq 140$ GPa. By comparison, the increased pressure on the surface of Venus is negligible (93 bars = 0.0093 GPa). Thus, under Venus conditions, the effects of the increased P on spectra are trivial, and the primary spectral changes will result from variations in T.

The temperature variation of Δ is expressed by Burns (1993) as:

$$\frac{\Delta_0}{\Delta_T} = \left(\frac{\Delta_0}{\Delta_T} \right)^{-5/3} = [1 - \alpha (T - T_0)]^{-5/3},$$

where α is the volume coefficient of thermal expansion, T is temperature, T_0 is ambient, and V and V_0 represent molar volumes at those temperatures. Interatomic distances increase as atoms grow farther apart as the result of increasing temperature. The net effect is that Δ decreases as T increases. This results in an inverse fifth power dependence of crystal field splitting (Δ) on cation-anion distance (R), expressed for the octahedral case as $\Delta \propto R^{-5}$ by Burns (1993). For high temperature spectra, there is also a general increase in the position of peak absorption intensity due to the enhanced thermal vibrations and enhanced vibronic coupling within each crystal site; see Burns (1982) and Burns (1993) for examples of such peak shifts in olivine group minerals.

In contrast, intervalence charge transfer phenomena, which also give rise to many features in the visible region, become more probable at high P because the sharing ions come closer together, but are decreased with increasing temperature, which pushes the ions farther apart. Oxygen-to-metal charge transfer features occur at the high end of the ultraviolet (UV)

portion of the spectrum but extend into the visible. These features are highly dependent on the specific coordination polyhedra studied, but they generally red-shift into the visible region at increasing temperatures. These general trends of peak shifts with changing T and P are summarized in Tables 9.2, 9.3, and 9.4 of Burns (1993), which include 42 papers (too numerous to list here) containing high temperature and/or high-pressure optical data published before 1992. A diminishing number of more recent papers have subsequently been published because our understanding of mantle phases has evolved and refocused on other types of spectroscopy.

This effect of temperature on NIR reflectance was discussed in the context of Venus by Pieters et al. (1986) who collected reflectance data of basaltic materials in the laboratory from 20°–500 °C. They found that with increasing temperature, the spectrum of hematite (and oxidized basalts) exhibited both a weakening of the Fe^{3+} crystal field absorption and a $\sim 0.1 \mu\text{m}$ shift of the Fe-O charge transfer absorption to longer wavelengths. Pieters et al. (1983) concluded that the relative brightness of hematite at 500 °C observed in the lab can explain the high reflectance of the Venus surface recorded by the $0.9 \mu\text{m}$ channel on Venera 9 and 10, consistent with the presence of ferric oxides on Venus and establishing the critical linkage between laboratory work and Venus observations. With the dawning age of Venus orbital spectroscopy, it is necessary to resume such laboratory measurements to understand spectral signatures as viewed from landers, descent imagers, and orbiters.

4.2.2 Venus Spectral Library Development

To address the need for high-temperature spectra, the Planetary Spectroscopy Laboratory (PSL) at DLR has created a novel facility dedicated to acquiring high-T emissivity data appropriate for interpretation of Venus surface spectra. The facility allows the collection of near to far-infrared emission spectroscopy ($0.7\text{--}200 \mu\text{m}$) of solid and powdered samples to temperatures up to 1000 K under medium vacuum conditions ($\sim 10\text{--}100 \text{ Pa}$) (Maturilli et al. 2018; Helbert et al. 2021). High temperature emissivity spectra for a set of natural mafic and felsic igneous rocks are shown in Fig. 11. Mafic materials have higher (by $\sim 30\%$) emissivity values than felsic materials, regardless of grain size, and can be readily distinguished even when subsampled to bands in the 5 atmospheric windows that permit nightside measurement of radiation emitted from the Venus surface (Fig. 12; Dyar et al. 2020, 2021; Helbert et al. 2021). These data confirm and allow quantification of the inverse relationship between FeO content and high-temperature emissivity (Dyar et al. 2020; Helbert et al. 2021). Helbert et al. (2021) applied this relationship directly to the spectrophotometer data collected by Venera 9 and 10, to show that FeO content of the rocks can be derived from the lander data and are consistent with basaltic compositions.

High temperature laboratory emissivity data, advancements in atmospheric characterization and modeling (Sect. 2.1), and improved knowledge of the surface temperature from topography are the cornerstones that allow derivation of surface composition from the nightside emissivity measurements to be taken by VERITAS, EnVision and DAVINCI orbiters and the dayside surface images to be collected by the DAVINCI probe. The expansion of the Venus spectral library critically enables the revolution in our understanding of surface mineralogy from the upcoming missions.

4.2.3 Spectral Measurements of Venus-Relevant Weathering Experiments

There are currently very limited spectroscopic measurements of weathered Venus analog materials and none, to date, measured spectroscopically at Venus temperatures. What little work has been analyzing VNIR reflectance spectroscopy on samples analyzed at Venus

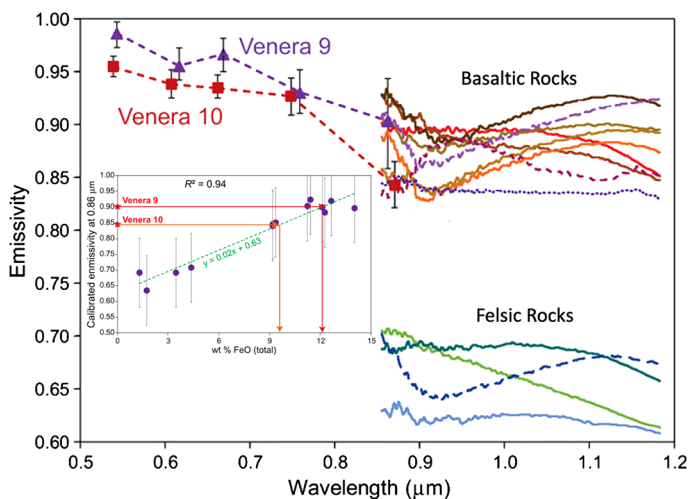


Fig. 11 Laboratory emissivity of geologic samples collected at 440 °C. Solid lines are solid samples and dashed lines are powders. The spectra are compared to reflectance data from the Venera 9 and 10 spectrophotometers (Ekonomov et al. 1980) converted to emissivity via Kirchhoff's Law (Helbert et al. 2021). Inset shows the relationship between emissivity and wt% FeO for laboratory and the Venera data. Modified from Helbert et al. (2021)

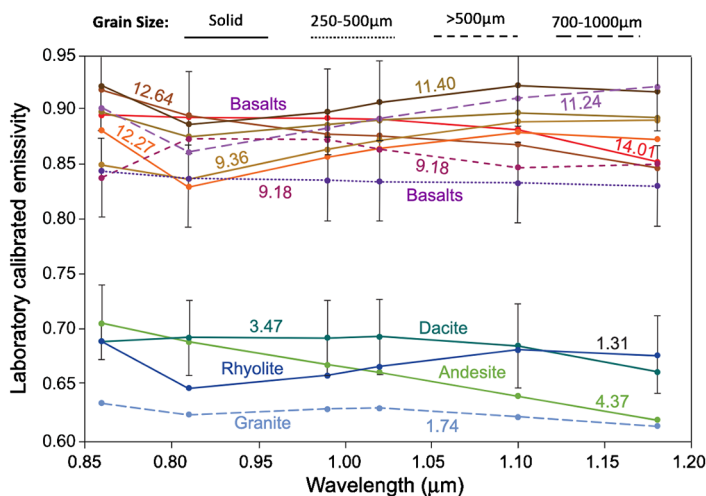


Fig. 12 Laboratory emissivity data of samples in Fig. 11 downsampled to 6 NIR bands sensitive to surface retrievals on Venus. Numbers are wt% FeO values of the samples, plotted in Fig. 11, inset. Error bars correspond to 4% estimated uncertainty of measurement from orbit. Modified from Helbert et al. (2021)

temperatures but under a terrestrial atmosphere (Filiberto et al. 2020; Cutler et al. 2020). Oxidation at Venus surface conditions forms discontinuous coatings of iron oxides mainly on glassy material and olivine crystals. Spectral measurements of these samples are consistent with first a flattening and reddening in the 1 μm region, consistent with the formation of magnetite first, before an increase in the reflectance and formation of new spectral features consistent with hematite. Limited high-temperature VNIR reflectance of Venus analog mate-

rials have also been recently done with a direct comparison of room temperature reflectance measurements (Treiman et al. 2021). This work has shown that at first order, the reflectance of igneous and sedimentary rocks are nearly identical except for the effects of oxidation on some surfaces. Basalt has reflectance near 7.5% and a leucogranite has reflectance near 50% (Treiman et al. 2021). Powdered hematite does shift its absorption edge slightly because it appears darker brown at high temperature (Yamanoi et al. 2009; Treiman et al. 2021).

There is clearly a need for more and diverse types of experiments to elucidate these interpretations, including measurement of altered surfaces at high temperatures. Such work is ongoing.

5 Summary

As with all planets, the mineralogy of the Venus surface provides a critical record of geologic and climatologic history and the current chemical exchanges between the atmosphere and solid body. In the absence of direct measurements of mineralogy, a range of approaches has been utilized to begin to constrain surface composition. Major element data from three Venera and Vega landers are consistent with tholeiitic or alkali basalts whose normative mineralogy can be calculated and serve as a starting point for comparison to other planets. The SO_3 content and density of these rocks indicate they have been altered under the current Venus atmosphere. Spectral reflectance from the Venera 9 and 10 photometers indicate oxidation, which is consistent with the range of f_{O_2} constrained by compositional and temperature measurements of the Venus atmosphere at specific altitudes, latitudes and time of day. Despite these limitations, thermodynamic modeling of equilibrium gas/surface chemistry provides a critical baseline for weathering reactions on Venus. These models show reactions driven primarily by sulfur chemistry and oxidation state, where Fe, Ca, Na, in minerals will convert to sulfates or sulfides (and/or oxides) as a function of S and O fugacity. The specifics and kinetics of these reactions are being investigated using experimental apparatus, ranging from low pressure, single gas experiments to the complex environment provided by the Glenn Extreme Environments Rig. These experiments, in concert with thermodynamic modeling, are essential to advancing our understanding of the stability and variety of minerals we can expect on the Venus surface.

The Venus Express mission demonstrated that surface emissivity through near-infrared windows in the CO_2 -rich atmosphere correlates with geomorphologic units, and provided, for the first time, a method to evaluate surface composition globally. The development of laboratory facilities to measure high temperature NIR emissivity of geologic materials has confirmed a relationship, predicted from theory, between emissivity and Fe^{2+} content in minerals. These measurements allow the community to develop a Venus spectral library that will prove essential for the interpretation of NIR data to be collected from the upcoming VERITAS, EnVision and DAVINCI missions and the ISRO Shukrayaan-1 (Haider et al. 2018; Sundararajan 2021) and Chinese Space Agency VOICE (Dong et al. 2023) missions in development. Spectral measurements of primary minerals and materials weathered under Venus conditions in the laboratory will strengthen our ability to recognize and infer mineralogy from these missions.

Reevaluation of the Magellan data also show spatial variability in the microwave emissivity of different terranes and locations on Venus. Microwave emissivity is related to the type and volume of high dielectric minerals in the rocks formed via igneous processes or through surface/atmosphere weathering reactions at varying temperatures. Laboratory measurements of the electrical properties of rocks at Venus temperatures and radar wavelengths

will facilitate our understanding these data, which provide an independent constraint on surface mineralogy that can be compared to the NIR data.

All of these approaches: theory, modeling, experiment and spectroscopy can and must be brought to bear collaboratively to understand the mineralogy and history of this Earth-sized world. But all of these rely heavily on direct, in situ measurements of the Venus environment: the chemistry and dynamics of the atmosphere via probe, balloon and orbit and the mineralogy of chemistry of surface rocks via landed assets such as the Roscosmos Venera-D mission in development (Senske et al. 2017; Zasova et al. 2019).

Acknowledgements Thanks to organizers of, participants in and conversations fostered by the International Space Science Institute “Venus: Evolution through Time” workshop, and to the patient editors of this volume.

Funding Open Access funding enabled and organized by Projekt DEAL.

Declarations

Competing Interests The authors declare no competing interests.

Open Access This article is licensed under a Creative Commons Attribution 4.0 International License, which permits use, sharing, adaptation, distribution and reproduction in any medium or format, as long as you give appropriate credit to the original author(s) and the source, provide a link to the Creative Commons licence, and indicate if changes were made. The images or other third party material in this article are included in the article’s Creative Commons licence, unless indicated otherwise in a credit line to the material. If material is not included in the article’s Creative Commons licence and your intended use is not permitted by statutory regulation or exceeds the permitted use, you will need to obtain permission directly from the copyright holder. To view a copy of this licence, visit <http://creativecommons.org/licenses/by/4.0/>.

References

- Abdrakhimov AM (2005) Geochemical comparison of volcanic rocks from terrestrial intraplate oceanic hot spots with Venusian surface material. *Geochem Int* 43:732–747
- Abdrakhimov AM, Basilevsky AT (2002) Geology of the Venera and Vega landing-site regions. *Sol Syst Res* 36:136–159
- Adams JB (1974) Visible and near-infrared diffuse reflectance spectra of pyroxenes as applied to remote sensing of solid objects in the solar system. *J Geophys Res* 79:4829–4836
- Akim EL, Stepanyantz VA (1993) Landing sites of automatic interplanetary probes on new map of Venus. Russian, *Astron Vestn*
- Arvidson RE et al (1994) Microwave signatures and surface properties of Ovda Regio and surroundings, Venus. *Icarus* 112:171–186. <https://doi.org/10.1006/icar.1994.1176>
- Asimow PD, Ghiorso MS (1998) Algorithmic modifications extending MELTS to calculate subsolidus phase relations. *Am Mineral* 83:1127–1131
- Aveline DC, Abbey WJ, Choukroun M, Treiman AH, Dyar MD, Smrekar SE, Feldman SM (2011) Rock and mineral weathering experiments under model Venus conditions. *Lunar Planet Sci Conf* 42:2165
- Baines KH et al (2000) Detection of sub-micron radiation from the surface of Venus by Cassini/VIMS. *Icarus* 148:307. <https://doi.org/10.1006/icar.2000.6519>
- Baker VR et al (1992) Channels and valleys on Venus: preliminary analysis of Magellan data. *J Geophys Res* 97:13421. <https://doi.org/10.1029/92JE00927>
- Barsukov VL, YuA S, Moskaleva LP et al (1982) Geochemical studies of the surface of Venus by the Venera 13 and 14 probes. *Geochem Int* 899–919
- Barsukov VL et al (1986) Geochemical studies on Venus with the landers from the Vega-1 and Vega-2 probes. *Geochem Int* 23:53–65
- Basilevsky AT (1993) Age of rifting and associated volcanism in Atla Regio, Venus. *Geophys Res Lett* 20:883–886. <https://doi.org/10.1029/93GL00736>
- Basilevsky AT et al (1985) The surface of Venus as revealed by the Venera landings: Part II. *Geol Soc Am Bull* 96:137–144

- Basilevsky AT, Nikolaeva OV, Weitz CM (1992) Geology of the Venera 8 landing site region from Magellan data: morphological and geochemical considerations. *J Geophys Res* 97:16315–16335
- Basilevsky AT, Head JW, Abdrakhimov AM (2004) Impact crater air fall deposits on the surface of Venus: areal distribution, estimated thickness, recognition in surface panoramas, and implications for provenance of sampled surface materials. *J Geophys Res* 109:E12003. <https://doi.org/10.1029/2004JE002307>
- Basilevsky AT et al (2007) Landing on Venus: past and future. *Planet Space Sci* 55:2097–2112
- Basilevsky AT et al (2012) Geologic interpretation of the near-infrared images of the surface taken by the Venus monitoring camera, Venus express. *Icarus* 217:434. <https://doi.org/10.1016/j.icarus.2011.11.003>
- Berger G et al (2019) Experimental exploration of volcanic rocks-atmosphere interactions under Venus surface conditions. *Icarus* 329:8–23. <https://doi.org/10.1016/j.icarus.2019.03.033>
- Brackett RA, Fegley B, Arvidson RE (1995) Volatile transport on Venus and implications for surface geochemistry and geology. *J Geophys Res* 100:1553–1563. <https://doi.org/10.1029/94JE02708>
- Bridges NT (1997) Ambient effects on basalt and rhyolite lavas under Venusian, subaerial, and subaqueous conditions. *J Geophys Res* 102:9243. <https://doi.org/10.1029/97JE00390>
- Brossier J, Gilmore MS (2021) Variations in the radiophysical properties of tesserae and mountain belts on Venus: classification and mineralogical trends. *Icarus* 355:114161. <https://doi.org/10.1016/j.icarus.2020.114161>
- Brossier J, Gilmore MS, Toner K (2020) Low radar emissivity signatures on Venus volcanoes and coronae: new insights on relative composition and age. *Icarus* 343:113693. <https://doi.org/10.1016/j.icarus.2020.113693>
- Brossier J et al (2021) Distinct mineralogy and age of individual lava flows in Atla Regio, Venus derived from Magellan radar emissivity. *J Geophys Res* 126:e2020JE006722. <https://doi.org/10.1029/2020JE006722>
- Brossier J, Gilmore MS, Head JW (2022) Extended rift-associated volcanism in Ganis Chasma, Venus detected from Magellan radar emissivity. *Geophys Res Lett* 49:e2022GL099765. <https://doi.org/10.1029/2022GL099765>
- Bullock MA, Grinspoon DH (1996) The stability of climate on Venus. *J Geophys Res* 101:7521. <https://doi.org/10.1029/95JE03862>
- Bullock MA, Grinspoon DH (2001) The recent evolution of climate on Venus. *Icarus* 150:19. <https://doi.org/10.1006/icar.2000.6570>
- Burns RG (1970) Mineralogical applications of crystal field theory. Cambridge University Press, Cambridge
- Burns RG (1982) Electronic spectra of minerals at high pressures: how the mantle excites electrons. In: Schreyer W (ed) High-pressure research in geosciences. E. Schweizerbart'sche Verlagsbuchhandlung, Stuttgart, pp 223–246
- Burns RG (1993) Mineralogical applications of crystal field theory, 2nd edn. Cambridge University Press, Cambridge
- Campbell BA (1994) Merging Magellan emissivity and SAR data for analysis of Venus surface dielectric properties. *Icarus* 112:187–203. <https://doi.org/10.1006/icar.1994.1177>
- Campbell BA (1995) Use and presentation of Magellan quantitative data in Venus mapping. USGS Open-File Report 95-519. <https://doi.org/10.3133/ofr95519>
- Campbell DB, Stacy NJS, Newman WI, Arvidson RE, Jones EM, Musser GS, Roper AY, Schaller C (1992) Magellan observations of extended impact crater related features on the surface of Venus. *J Geophys Res* 97:16249–16277. <https://doi.org/10.1029/92je01634>
- Campbell BA, Campbell DB, Morgan GA et al (2015) Evidence for crater ejecta on Venus tessera terrain from Earth-based radar images. *Icarus* 250:123–130. <https://doi.org/10.1016/j.icarus.2014.11.025>
- Campbell BA, Morgan GA, Whitten JL et al (2017) Pyroclastic flow deposits on Venus as indicators of renewed magmatic activity. *J Geophys Res* 122:1580–1596. <https://doi.org/10.1002/2017je005299>
- Carrier WD et al (1991) Physical properties of the lunar surface. In: Heiken GH, Vaniman DT, French BM (eds) Lunar sourcebook, a user's guide to the moon. Cambridge University Press, Cambridge
- Cloutis EA, Gaffey MJ (1991) Pyroxene spectroscopy revisited: spectral-compositional correlations and relationship to geothermometry. *J Geophys Res* 96:22809–22826
- Cross W, Iddings JP, Pirsson LV, Washington HS (1902) A quantitative chemicominalogical classification and nomenclature of igneous rocks. *J Geol* 10:555–690
- Cutler KS, Filiberto J, Treiman AH, Trang D (2020) Experimental investigation of oxidation of pyroxene and basalt: implications for spectroscopic analyses of the surface of Venus and the ages of lava flows. *Planet Space Sci* 1:21
- D'Incecco P, Müller N, Helbert J, D'Amore M (2017) Idunn Mons on Venus: location and extent of recently active lava flows. *Planet Space Sci* 136:25–33. <https://doi.org/10.1016/j.pss.2016.12.002>
- D'Incecco P, Filiberto J, López I, Gorinov DA, Komatsu G (2021) Idunn Mons: evidence for ongoing volcano-tectonic activity and atmospheric implications on Venus. *Planet Space Sci* 2:215
- Dong X, Liu Y, He J (2023) VOICE: a Venus Volcano Imaging and Climate Explorer mission. *LPI Contributions* 2807, 8068. <https://ui.adsabs.harvard.edu/abs/2023LPICo2807.8068D>

- Dyar MD et al (2020) Probing Venus surface iron contents with six-band visible near-infrared spectroscopy from orbit. *Geophys Res Lett* 47:e2020GL090497. <https://doi.org/10.1029/2020GL090497>
- Dyar MD et al (2021) Surface weathering on Venus: constraints from kinetic, spectroscopic, and geochemical data. *Icarus* 358:114139. <https://doi.org/10.1016/j.icarus.2020.114139>
- Ekonomov AP (2015) Resolving the surface details on Venus in the balloon- or lander-borne images with a computer modeling method. *Sol Syst Res* 49:110. <https://doi.org/10.1134/S003809461502001X>
- Ekonomov AP, YuM G, Moshkin BE (1980) Visible radiation observed near the surface of Venus: results and their interpretation. *Icarus* 41:65–75. [https://doi.org/10.1016/0019-1035\(80\)90159-1](https://doi.org/10.1016/0019-1035(80)90159-1)
- Fagents S, Greeley R (2001) Factors influencing lava-substrate heat transfer and implications for thermomechanical erosion. *Bull Volcanol* 62:519. <https://doi.org/10.1007/s004450000113>
- Fedorova A et al (2015) The CO₂ continuum absorption in the 1.10- and 1.18- μ m windows on Venus from Maxwell Montes transits by SPICAV IR onboard Venus express. *Planet Space Sci* 113:66. <https://doi.org/10.1016/j.pss.2014.08.010>
- Fegley B Jr, Prinn RG (1989) Estimation of the rate of volcanism on Venus from reaction rate measurements. *Nature* 337:55–58. <https://doi.org/10.1038/337055a0>
- Fegley B (2003) Venus. In: Holland HD, Turekian KK (eds) *Treatise on geochemistry*, vol 1. Elsevier, pp 487–507. <https://doi.org/10.1016/b0-08-043751-6/01150-6>
- Fegley BK, Lodders K, Treiman AH, Klingelhöfer G (1995) The rate of pyrite decomposition on the surface of Venus. *Icarus* 115:159–180. <https://doi.org/10.1006/icar.1995.1086>
- Filiberto J (2014) Magmatic diversity on Venus: constraints from terrestrial analog crystallization experiments. *Icarus* 231:131–136. <https://doi.org/10.1016/j.icarus.2013.12.003>
- Filiberto J et al (2020) Present-day volcanism on Venus as evidenced from weathering rates of olivine. *Sci Adv* 6:aax7445. <https://doi.org/10.1126/sciadv.aax7445>
- Fink JH, Bridges NT, Grimm RE (1993) Shapes of Venusian “pancake” domes imply episodic emplacement and silicic composition. *Geophys Res Lett* 20:261. <https://doi.org/10.1029/92GL03010>
- Fink JH, Anderson SW (1999) Lava domes and Coulées. In: Sigurdsson H et al (eds) *Encyclopedia of volcanoes*. Academic, New York, pp 307–319
- Florensky CP et al (1977b) The surface of Venus as revealed by Soviet Venera 9 and 10. *Geol Soc Am Bull* 88:1537. [https://doi.org/10.1130/0016-7606\(1977\)88<1537:TSOVAR>2.0.CO;2](https://doi.org/10.1130/0016-7606(1977)88<1537:TSOVAR>2.0.CO;2)
- Florensky CP, Ronca LB, Basilevsky AT (1977a) Geomorphic degradations on the surface of Venus: an analysis of Venera 9 and Venera 10 data. *Science* 196:869–871. <https://doi.org/10.1126/science.196.4292.869>
- Florensky CP et al (1983a) The oxidizing-reducing conditions on the surface of Venus according to the data of the “KONTRAST” geochemical indicator on the Venera 13 and Venera 14 spacecraft. *Cosm Res* 21:278–281
- Florensky CP et al (1983b) Venera 13 and Venera 14: sedimentary rocks on Venus? *Science* 221:57–59. <https://doi.org/10.1126/science.221.4605.57>
- Ford PG, Pettengill GH (1983) Venus: global surface radio emissivity. *Science* 220:1379–1381. <https://doi.org/10.1126/science.220.4604.1379>
- Garvin JB, Head JW, Wilson L (1982) Magma vesiculation and pyroclastic volcanism on Venus. *Icarus* 52:365–372. [https://doi.org/10.1016/0019-1035\(82\)90119-1](https://doi.org/10.1016/0019-1035(82)90119-1)
- Garvin JB et al (1984) Venus: the nature of the surface from Venera panoramas. *J Geophys Res* 89:3381–3399. <https://doi.org/10.1029/JB089iB05p03381>
- Garvin JB, Head JW, Pettengill GH, Zisk SH (1985) Venus global radar reflectivity and correlations with elevation. *J Geophys Res* 90:6859
- Garvin JB et al (2022) Revealing the mysteries of Venus: the DAVINCI mission. *Planet Sci J* 3:117
- Ghiorso MS, Sack RO (1995) Chemical mass transfer in magmatic processes. IV. A revised and internally consistent thermodynamic model for the interpolation and extrapolation of liquid-solid equilibria in magmatic systems at elevated temperatures and pressures. *Contrib Mineral Petrol* 119:197–212
- Gilmore MS, Head JW (2000) Sequential deformation of plains at the margins of Alpha Regio, Venus: implications for tessera formation. *Meteorit Planet Sci* 35:667–687. <https://doi.org/10.1111/j.1945-5100.2000.tb01451.x>
- Gilmore M, Mueller N, Helbert J (2015) VIRTIS emissivity of Alpha Regio, Venus, with implications for tessera composition. *Icarus* 254:350–361. <https://doi.org/10.1016/j.icarus.2015.04.008>
- Gilmore MS et al (2017) Venus surface composition constrained by observation and experiment. *Space Sci Rev* 212:1–30. <https://doi.org/10.1007/s11214-017-0370-8>
- Giordano D, Russell JK, Dingwell DB (2008) Viscosity of magmatic liquids: a model. *Earth Planet Sci Lett* 27:123. <https://doi.org/10.1016/j.epsl.2008.03.038>
- Golovin YM, Moshkin BY, Ekonomov AP (1983) Some optical properties of the Venus surface. In: *Venus*, p 131136

- Greaves JS et al (2020) Phosphine gas in the cloud decks of Venus. *Nat Astron* 1–20. <https://doi.org/10.1038/s41550-020-1174-4>
- Greeley R et al (1992) Aeolian features on Venus: preliminary Magellan results. *J Geophys Res* 97:13319–13345. <https://doi.org/10.1029/92JE00980>
- Gregg TKP, Greeley R (1993) Formation of venusian canali: considerations of lava types and their thermal behaviors. *J Geophys Res* 98:10873. <https://doi.org/10.1029/93JE00692>
- Hagfors T (1970) Remote probing of the moon by infrared and microwave emissions and by radar. *Radio Sci* 5:189–227
- Haider SA, Bhardwaj A, Shanmugam M, Goyal SK, Sheel V, Pabari J, Prasad Karanam D (2018) Indian Mars and Venus missions: science and exploration. 42nd COSPAR Scientific Assembly 42:B4-1
- Hashimoto GL, Imamura T (2001) Elucidating the rate of volcanism on Venus: detection of lava eruptions using near-infrared observations. *Icarus* 154:239. <https://doi.org/10.1006/icar.2001.6713>
- Hashimoto GL, Sugita S (2003) On observing the compositional variability of the surface of Venus using nightside near-infrared thermal radiation. *J Geophys Res* 108:5109. <https://doi.org/10.1029/2003JE002082>
- Hashimoto GL et al (2008) Felsic highland crust on Venus suggested by Galileo near-infrared mapping spectrometer data. *J Geophys Res* 113:E00B24. <https://doi.org/10.1029/2008JE003134>
- Haus R, Arnold G (2010) Radiative transfer in the atmosphere of Venus and application to surface emissivity retrieval from VIRTIS/VEX measurements. *Planet Space Sci* 5:1578. <https://doi.org/10.1016/j.pss.2010.08.001>
- Havinga EE (1961) The temperature dependence of dielectric constants. *J Phys Chem Solids* 18:253–255. [https://doi.org/10.1016/0022-3697\(61\)90169-X](https://doi.org/10.1016/0022-3697(61)90169-X)
- Head JW, Wilson L (1986) Volcanic processes and landforms on Venus: theory, predictions, and observations. *J Geophys Res* 91:9407. <https://doi.org/10.1029/JB091iB09p09407>
- Head JW et al (1992) Venus volcanism: classification of volcanic features and structures, associations, and global distribution from Magellan data. *J Geophys Res* 97:13153. <https://doi.org/10.1029/92JE01273>
- Helbert J et al (2008) Surface brightness variations seen by VIRTIS on Venus express and implications for the evolution of the Lada Terra region, Venus. *Geophys Res Lett* 35:L11201. <https://doi.org/10.1029/2008GL033609>
- Helbert J, Säuberlich T, Dyar MD et al (2020) The Venus Emissivity Mapper (VEM): advanced development status and performance evaluation. In: *Proc SPIE* 11502, infrared remote sensing and instrumentation XXVIII, 20 August 2020, vol 1150208. <https://doi.org/10.1117/12.2567634>
- Helbert J et al (2021) Deriving iron contents from past and future Venus surface spectra with new high-temperature laboratory emissivity data. *Sci Adv* 7:eaba9428. <https://doi.org/10.1126/sciadv.aba9428>
- Herrick RR, Hensley S (2023) Surface changes observed on a Venusian volcano during the Magellan mission. *Science* 379:1205–1208. <https://doi.org/10.1126/science.abm7735>
- Johnson NM, Fegley B Jr (2000) Water on Venus: new insights from tremolite decomposition. *Icarus* 146:301–306
- Johnson NM, Fegley B Jr (2002) Tremolite decomposition and Venus. *Meteorit Plan Sci Suppl* 37:A72
- Johnson NM, Fegley B Jr (2003) Tremolite decomposition on Venus II. Products, kinetics, and mechanism. *Icarus* 164:317–333
- Kadlec F et al (2011) Study of the ferroelectric phase transition in germanium telluride using time-domain terahertz spectroscopy. *Phys Rev B* 84:205. <https://doi.org/10.1103/PhysRevB.84.205209>
- Kappel D, Haus R, Arnold G (2015) Error analysis for retrieval of Venus' IR surface emissivity from VIRTIS/VEX measurements. *Planet Space Sci* 113–114:49–65. <https://doi.org/10.1016/j.pss.2015.01.014>
- Kappel D, Arnold G, Haus R (2016) Multi-spectrum retrieval of Venus IR surface emissivity maps from VIRTIS/VEX nightside measurements at Themis Regio. *Icarus* 265:42. <https://doi.org/10.1016/j.icarus.2015.10.014>
- Kargel JS et al (1993) The volcanology of Venera and VEGA landing sites and the geochemistry of Venus. *Icarus* 103:253–275. <https://doi.org/10.1006/icar.1993.1069>
- Kargel JS et al (1994) Carbonate-sulfate volcanism on Venus? *Icarus* 112:219. <https://doi.org/10.1006/icar.1994.1179>
- Khodakovskiy IL, Volkov VP, Sidorov YI, Borisov MV, Lomonosov MV (1979) Venus: preliminary prediction of the mineral composition of surface rocks. *Icarus* 39:352–363
- Kilburn C (2000) Lava flows. In: Sigurdsson H et al (eds) *Encyclopedia of volcanoes*. Academic, New York, pp 291–306
- King PL, Wheeler VW, Renggli CJ, Palm AB, Wilson S, Harrison AL, Morgan B, Nekvasil H, Troitzsch U, Mernagh T, Yue L (2018) Gas–solid reactions: theory, experiments and case studies relevant to Earth and planetary processes. *Rev Mineral Geochem* 84:1–56
- Klose KB, Zolotov MY (1992) Chemical weathering of evolved igneous rocks on Venus. *Lunar Plan Sci Conf* 23

- Klose KB, Wood JA, Hashimoto A (1992) Mineral equilibria and the high radar reflectivity of Venus mountaintops. *J Geophys Res* 97:16353–16369. <https://doi.org/10.1029/92JE01865>
- Knafele J et al (2019) The effect of oxidation on the mineralogy and magnetic properties of olivine. *Am Mineral* 104:694–702
- Knically J, Herrick RR (2020) Evaluation of the bandwidths and spatial resolutions achievable with near-infrared observations of Venus below the cloud deck. *Planet Space Sci* 181:104787. <https://doi.org/10.1016/j.pss.2019.104787>
- Kohler E (2016) Investigating mineral stability under Venus conditions: a focus on the Venus radar anomalies. Theses and Dissertations
- Kohler E et al (2015) Radar-reflective minerals investigated under Venus near-surface conditions. *Lunar Plan Sci Conf* 46:2563
- Komatsu G et al (1993) Venusian channels and valleys: distribution and volcanological implications. *Icarus* 102:1. <https://doi.org/10.1006/icar.1993.1029>
- Le Voyer M et al (2019) Carbon fluxes and primary magma CO₂ contents along the global mid-ocean ridge system. *Geochem Geophys Geosyst* 20:1387–1424. <https://doi.org/10.1029/2018GC007630>
- Lebonnois S, Schubert G (2017) The deep atmosphere of Venus and the possible role of density-driven separation of CO₂ and N₂. *Nat Geosci* 10:473. <https://doi.org/10.1038/ngeo2971>
- Lebonnois S et al (2018) Planetary boundary layer and slope winds on Venus. *Icarus* 314:149. <https://doi.org/10.1016/j.icarus.2018.06.006>
- Lecacheux J et al (1993) Detection of the surface of Venus at 1.0 μ m from ground-based observations. *Planet Space Sci* 41:543. [https://doi.org/10.1016/0032-0633\(93\)90035-Z](https://doi.org/10.1016/0032-0633(93)90035-Z)
- Lejeune A-M, Richet P (1995) Rheology of crystal-bearing silicate melts: an experimental study at high viscosities. *J Geophys Res* 100:4215. <https://doi.org/10.1029/94JB02985>
- López I, D'Incecco P, Filiberto J, Komatsu G (2022) The volcanology of Idunn Mons, Venus: the complex evolution of a possible active volcano. *J Volcanol Geotherm Res* 421:107428
- Lorenz RD, Crisp D, Huber L (2018) Venus atmospheric structure and dynamics from the VEGA lander and balloons: new results and PDS archive. *Icarus* 305:277–283. <https://doi.org/10.1016/j.icarus.2017.12.044>
- Marov MY, Grinspoon DH (1998) The planet Venus. Yale University Press, New Haven
- Masursky H et al (1980) Pioneer Venus radar results: geology from images and altimetry. *J Geophys Res* 85:8232–8260. <https://doi.org/10.1029/JA085iA13p08232>
- Maturilli A et al (2018) The Planetary Spectroscopy Laboratory (PSL): wide spectral range, wider sample temperature range. In: *Proc. SPIE* 10765, infrared remote sensing and instrumentation XXVI:107650A. <https://doi.org/10.1117/12.2319944>
- McCanta MC, Dyar MD, Treiman AH (2014) Alteration of Hawaiian basalts under sulfur-rich conditions: applications to understanding surface-atmosphere interactions on Mars and Venus. *Am Mineral* 99:291–302. <https://doi.org/10.2138/am.2014.4584>
- McEwen AS, Keszthelyi L, Geissler P, Simonelli DP, Carr MH, Johnson TV, Klaasen KP, Breneman HH, Jones TJ, Kaufman JM, Magee KP (1998) Active volcanism on Io as seen by Galileo SSI. *Icarus* 135:181–219
- Meadows VS, Crisp D (1996) Ground-based near-infrared observations of the Venus nightside: the thermal structure and water abundance near the surface. *J Geophys Res* 101:4595. <https://doi.org/10.1029/95JE03567>
- Moore HJ et al (1992) An unusual volcano on Venus. *J Geophys Res* 97:13479. <https://doi.org/10.1029/92JE00957>
- Moroz VI (1983) Summary of preliminary results of the Venera 13 and Venera 14 missions. In: *Venus*. University of Arizona Press, Tucson, pp 45–68
- Moroz VI (2002) Estimates of visibility of the surface of Venus from descent probes and balloons. *Planet Space Sci* 50:287. [https://doi.org/10.1016/S0032-0633\(01\)00128-3](https://doi.org/10.1016/S0032-0633(01)00128-3)
- Morris RV, Lauer HV, Lawson C, Gibson EK, Nace GA, Stewart C (1985) Spectral and other physicochemical properties of submicron powders of hematite (α -Fe₂O₃), maghemite (γ -Fe₂O₃), magnetite (Fe₃O₄), goethite (α -FeOOH), and lepidocrocite (γ -FeOOH). *J Geophys Res* 90:3126–3144. <https://doi.org/10.1029/jb090i04p03126>
- Mueller N et al (2008) Venus surface thermal emission at 1 μ m in VIRTIS imaging observations: evidence for variation of crust and mantle differentiation conditions. *J Geophys Res* 113:E00B17. <https://doi.org/10.1029/2008JE003118>
- Mueller NT et al (2018) Regional Venus surface temperature variations in models and infrared observations. *Lunar Plan Sci Conf* 49:2400
- Mueller NT, Smrekar SE, Tsang CCC (2020) Multispectral surface emissivity from VIRTIS on Venus express. *Icarus* 335:113400. <https://doi.org/10.1016/j.icarus.2019.113400>










- Nikolaeva OV (1990) Geochemistry of the Venera 8 material demonstrates the presence of continental crust on Venus. *Earth Moon Planets* 50/51:329–341. <https://doi.org/10.1007/BF00142398>
- Nikolaeva OV (1995) K-U-Th systematics of terrestrial magmatic rocks for planetary comparisons: terrestrial N-MORBs and venusian basaltic material. *Geochem Int* 33:1–11
- Nikolaeva OV (1997) K-U-Th systematics of igneous rocks for planetological comparisons: oceanic island-arc volcanics on Earth versus rocks on the surface of Venus. *Geochem Int* 35:424–447
- Noack L, Breuer D, Spohn T (2012) Coupling the atmosphere with interior dynamics: implications for the resurfacing of Venus. *Icarus* 217:484. <https://doi.org/10.1016/j.icarus.2011.08.026>
- Olhoeft GR, Strangway DW (1975) Dielectric properties of the first 100 meters of the moon. *Earth Planet Sci Lett* 24:394–404
- Oshigami S, Namiki N (2007) Cross-sectional profiles of Baltis Vallis channel on Venus: reconstructions from Magellan SAR brightness data. *Icarus* 190:1. <https://doi.org/10.1016/j.icarus.2007.03.011>
- Oshigami S, Namiki N, Komatsu G (2009) Depth profiles of venusian sinuous rilles and valley networks. *Icarus* 199:250. <https://doi.org/10.1016/j.icarus.2008.10.012>
- Pavri B et al (1992) Steep-sided domes on Venus: characteristics, geologic setting, and eruption conditions from Magellan data. *J Geophys Res* 97:13445. <https://doi.org/10.1029/92JE01162>
- Pettengill GH, Ford PG, Chapman BD (1988) Venus: electromagnetic properties. *J Geophys Res* 93:14881–14892. <https://doi.org/10.1029/JB093iB12p14881>
- Pettengill GH, Ford PG, Wilt RJ (1992) Venus surface radiothermal emission as observed by Magellan. *J Geophys Res* 97:13091–13102. <https://doi.org/10.1029/92JE01356>
- Pettengill GH, Ford PG, Simpson RA (1996) Electrical properties of the Venus surface from bistatic radar observations. *Science* 272:1628–1631. <https://doi.org/10.1126/science.272.5268.1628>
- Pieters CM et al (1983) Strength of mineral absorption features in the transmitted component of near-infrared reflected light: first results from RELAB. *J Geophys Res* 88:9534–9544. <https://doi.org/10.1029/JB088iB11p09534>
- Pieters CM et al (1986) The color of the surface of Venus. *Science* 234:1379–1383. <https://doi.org/10.1126/science.234.4782.1379>
- Pollack JB, Dalton JB, Grinspoon D et al (1993) Near-infrared light from Venus' nightside: a spectroscopic analysis. *Icarus* 103:1–42. <https://doi.org/10.1006/icar.1993.1055>
- Port ST, Chevrier VF (2020) Stability of pyrrhotite under experimentally simulated Venus conditions. *Planet Space Sci* 105022. <https://doi.org/10.1016/j.pss.2020.105022>
- Port ST, Chevrier VF (2021) Numerical investigation of Mercury-bearing minerals to address the low emissivity anomaly on the highlands of Venus. *Lunar Plan Sci Conf* 52:2548
- Port ST, Kohler E, Craig PI, Chevrier V (2016) Stability of pyrite under Venusian surface conditions. *Lunar Planet Sci* 47:2144
- Port ST, Chevrier VF, Kohler E (2020) Investigation into the radar anomaly on Venus: the effect of Venus conditions on bismuth, tellurium, and sulfur mixtures. *Icarus* 336:113432. <https://doi.org/10.1016/j.icarus.2019.113432>
- Radoman-Shaw BG, Harvey RP, Costa G et al (2022) Experiments on the reactivity of basaltic minerals and glasses in Venus surface conditions using the Glenn Extreme Environment Rig. *Meteorit Planet Sci.* <https://doi.org/10.1111/maps.13902>
- Ragent B et al (1985) Particulate matter in the Venus atmosphere. *Adv Space Res* 5:85. [https://doi.org/10.1016/0273-1177\(85\)90199-1](https://doi.org/10.1016/0273-1177(85)90199-1)
- Reid RB (2021) Experimental alteration of venusian surface basalts in a hybrid CO₂-SO₂ atmosphere. Masters thesis, Univ. Tennessee
- Roberts JJ, Tyburczy JA (1991) Frequency dependent electrical properties of polycrystalline olivine compacts. *J Geophys Res* 96:16205–16222
- Robinson CA, Wood JA (1993) Recent volcanic activity on Venus: evidence from radiothermal emissivity measurements. *Icarus* 102:26–39. <https://doi.org/10.1006/icar.1993.1030>
- Santos AR, Gilmore MS, Greenwood JP, Nakley LM, Phillips K, Kremic T, Lopez X (2023) Experimental weathering of rocks and minerals at Venus conditions in the Glenn Extreme Environments Rig (GEER). *J Geophys Res.* <https://doi.org/10.1029/2022JE007423>
- Schaefer L, Fegley B (2004) Heavy metal frost on Venus. *Icarus* 168:215–219. <https://doi.org/10.1016/j.icarus.2003.11.023>
- Seiff A (1987) Further information on structure of the atmosphere of Venus derived from the VEGA Venus Balloon and Lander mission. *Adv Space Res* 7:323–328. [https://doi.org/10.1016/0273-1177\(87\)90239-0](https://doi.org/10.1016/0273-1177(87)90239-0)
- Seiff A, Schofield JT, Kliore AJ et al (1985) Models of the structure of the atmosphere of Venus from the surface to 100 kilometers altitude. *Adv Space Res* 5:3–58. [https://doi.org/10.1016/0273-1177\(85\)90197-8](https://doi.org/10.1016/0273-1177(85)90197-8)
- Selivanov AS, Gektin YM, Naraeva MK, Panfilov AS, Fokin AB (1982) Evolution of the VENERA-13 imagery. *Sov Astron Lett* 8:235–236

- Semprich J, Filiberto J, Treiman AH (2020) Venus: a phase equilibria approach to model surface alteration as a function of rock composition, oxygen- and sulfur fugacities. *Icarus* 346:113779. <https://doi.org/10.1016/j.icarus.2020.113779>
- Senske DA, Zasova LV, Ignatiev NI et al (2017) Venera-D: Expanding our horizon of terrestrial planet climate and geology through the comprehensive exploration of Venus. Report of the Venera-D Joint Science Definition Team
- Shalygin EV et al (2015) Active volcanism on Venus in the Ganiki Chasma rift zone. *Geophys Res Lett* 42:4762–4769. <https://doi.org/10.1002/2015GL064088>
- Shellnutt JG (2013) Petrological modeling of basaltic rocks from Venus: a case for the presence of silicic rocks. *J Geophys Res, Planets* 118:1350–1364. <https://doi.org/10.1002/jgre.20094>
- Shellnutt JG (2018) Derivation of intermediate to silicic magma from the basalt analyzed at the Vega 2 landing site, Venus. *PLoS ONE* 13:e0194155
- Shepard MK et al (1994) A ferroelectric model for the low emissivity highlands on Venus. *Geophys Res Lett* 21:469–472. <https://doi.org/10.1029/94GL00392>
- Smrekar SE (1994) Evidence for active hotspots on Venus from analysis of Magellan gravity data. *Icarus* 112:2–26. <https://doi.org/10.1006/icar.1994.1166>
- Smrekar SE et al (2010) Recent hotspot volcanism on Venus from VIRTIS emissivity data. *Science* 328:605–608. <https://doi.org/10.1126/science.1186785>
- Snels M et al (2021) A simulation chamber for absorption spectroscopy in planetary atmospheres. *Atmos Meas Tech* 14:7187. <https://doi.org/10.5194/amt-14-7187-2021>
- Snyder D (2002) Cooling of lava flows on Venus: the coupling of radiative and convective heat transfer. *J Geophys Res* 107:5080. <https://doi.org/10.1029/2001JE001501>
- Stofan ER et al (1995) Large topographic rises on Venus: implications for mantle upwellings. *J Geophys Res* 327:317–323. <https://doi.org/10.1029/95JE01834>
- Stofan ER et al (2000) Emplacement and composition of steep-sided domes on Venus. *J Geophys Res* 105:26757. <https://doi.org/10.1029/1999JE001206>
- Stofan ER, Smrekar SE, Mueller N, Helbert J (2016) Themis regio, Venus: evidence for recent (?) volcanism from VIRTIS data. *Icarus* 271:375–386. <https://doi.org/10.1016/j.icarus.2016.01.034>
- Strezoski A, Treiman AH (2022) The “Snow Line” on Venus’s Maxwell Montes: varying elevation implies a dynamic atmosphere. *Planet Sci J* 3:264. <https://doi.org/10.3847/PSJ/ac9f3a>
- Subbarao EC (1973) Ferroelectric and antiferroelectric materials. *Ferroelectrics* 5:267–280
- Sundararajan V (2021) Tradespace exploration of space system architecture and design for India’s Shukrayaan-1, Venus orbiter mission. In: ASCEND 2021, p 4103
- Surkov YA et al (1977) Density of surface rock on Venus from data obtained by the Venera 10 automatic interplanetary station. *Cosm Res* 14:612–618
- Surkov YA et al (1984) New data on the composition, structure, and properties of Venus rock obtained by Venera 13 and 14. *J Geophys Res* 89:B393–B402. <https://doi.org/10.1029/JB089iS02p0B393>
- Surkov YA et al (1986) Venus rock composition at the Vega 2 landing site. *J Geophys Res* 91:E215. <https://doi.org/10.1029/JB091iB13p0E215>
- Surkov YA, Kirnozov FF, Glazov VN (1987) Uranium, thorium, and potassium in the Venusian rocks at the landing sites of Vega 1 and 2. *J Geophys Res* 92:E537–E540. <https://doi.org/10.1029/JB092iB04p0E537>
- Teffetteller H et al (2022) An experimental study of the alteration of basalt on the surface of Venus. *Icarus* 384:115085. <https://doi.org/10.1016/j.icarus.2022.115085>
- Treiman AH (1994) Comment on “Formation of Venusian canali: Considerations of lava types and their thermal behaviors” by Gregg, T. K. P. and Greeley, R.. *J Geophys Res* 99:17163. <https://doi.org/10.1029/93JE03576>
- Treiman AH (2007) Geochemistry of Venus’ surface: current limitations as future opportunities. In: Esposito LW, Stofan ER, Cravens TE (eds) *Exploring Venus as a terrestrial planet*. <https://doi.org/10.1029/176GM03>
- Treiman AH, Schwenzer SP (2009) Basalt–atmosphere interaction on Venus: preliminary results on weathering of minerals and bulk rock. In: *Venus geochemistry: progress, prospects, and new missions*, 26–27 Feb 2009. Houston, TX, USA
- Treiman A, Harrington E, Sharpton V (2016) Venus’ radar-bright highlands: different signatures and materials on Ovda Regio and on Maxwell Montes. *Icarus* 280:172–182. <https://doi.org/10.1016/j.icarus.2016.07.001>
- Treiman AH, Filiberto J, Kaaden KEV (2021) Near-infrared reflectance of rocks at high temperature: preliminary results and implications for near-infrared emissivity of Venus’s surface. *Plan Sci J* 2:43. <https://doi.org/10.3847/PSJ/abd546>
- Truong N, Lunine JJ (2021) Volcanically extruded phosphides as an abiotic source of Venusian phosphine. *Proc Natl Acad Sci* 118:e2021689118. <https://doi.org/10.1073/pnas.2021689118>

- Venera-D Joint Science Definition Team (JSDT) (2017) Venera-D: Expanding our Horizon of Terrestrial Planet Climate and Geology through the Comprehensive Exploration of Venus. <https://www.lpi.usra.edu/vexag/meetings/meetings-of-interest/Venera-D-Report.pdf>
- Volkov VP, Zolotov MY, Khodakovskiy IL (1986) Lithospheric-atmospheric interaction on Venus. In: Saxena SK (ed) Chemistry and physics of terrestrial planets. Springer, New York, pp 136–190. https://doi.org/10.1007/978-1-4612-4928-3_4
- Weitz CM, Basilevsky AT (1993) Magellan observations of the Venera and Vega landing site regions. *J Geophys Res* 98:17069
- Widemann T, Ghail R, Wilson C, Titov D (2021) EnVision at Venus: Europe's next medium-class science mission. 19th Meeting of the Venus Exploration Analysis Group. Abstract #8068
- Williams DA, Kerr RC, Leshner CM, Barnes SJ (2001) Analytical/numerical modeling of komatiite lava emplacement and thermal erosion at Perseverance, Western Australia. *J Volcanol Geotherm Res* 110:27–55. [https://doi.org/10.1016/S0377-0273\(01\)00206-2](https://doi.org/10.1016/S0377-0273(01)00206-2)
- Williams-Jones G, Williams-Jones AE, Stix J (1998) The nature and origin of Venusian canali. *J Geophys Res* 103:8545–8555. <https://doi.org/10.1029/98JE00243>
- Wilt JR (1992) A study of areas of low radio-thermal emissivity on Venus. PhD thesis, Massachusetts Institute of Technology, Cambridge
- Wood JA, Brett R (1997) Comment on “The rate of pyrite decomposition on the surface of Venus”. *Icarus* 128:472–473. <https://doi.org/10.1006/icar.1997.5743>
- Wood BE et al (2022) Parker Solar Probe imaging of the night side of Venus. *Geophys Res Lett* 49:e96302. <https://doi.org/10.1029/2021GL096302>
- Wroblewski FB et al (2019) Ovda Fluctus, the festoon lava flow on Ovda Regio, Venus: not silica-rich. *J Geophys Res* 124:2233. <https://doi.org/10.1029/2019JE006039>
- Yamanoi Y, Nakashima S, Katsura M (2009) Temperature dependence of reflectance spectra and color values of hematite by in situ, high-temperature visible micro-spectroscopy. *Am Mineral* 94:90–97. <https://doi.org/10.2138/am.2009.2779>
- Young KF, Frederikse HPR (1973) Compilation of the static dielectric constant of inorganic solids. *J Phys Chem Ref Data* 2:313. <https://doi.org/10.1063/1.3253121>
- Zasova LV, Gorinov DA, Eismont NA et al (2019) Venera-D: a design of an automatic space station for Venus exploration. *Sol Syst Res* 53:506–510. <https://doi.org/10.1134/S0038094619070244>
- Zhong S-S et al (2023) High temperature oxidation of magnesium- and iron-rich olivine under a CO₂ atmosphere: implications for Venus. *Remote Sens* 15:1959. <https://doi.org/10.3390/rs15081959>
- Zolotov MY (1994) Phase relations in the Fe-Ti-Mg-O oxide system and hematite stability at the condition of Venus'. *Surface Lunar Plan Sci Conf* 25
- Zolotov MY (2007) Solid planet-atmosphere interactions. In: Schubert G (ed) *Treatise on Geophysics*, vol 10. Elsevier, pp 349–369. <https://doi.org/10.1016/B978-0-444-52748-6.00181-4>
- Zolotov MY (2018) Gas–solid interactions on Venus and other solar system bodies. *Rev Mineral Geochem* 84:351–392. <https://doi.org/10.2138/rmg.2018.84.10>

Publisher's Note Springer Nature remains neutral with regard to jurisdictional claims in published maps and institutional affiliations.

Authors and Affiliations

Martha S. Gilmore¹  · M. Darby Dyar^{2,3}  · Nils Mueller⁴  · Jérémy Brossier⁵  · Alison R. Santos¹  · Mikhail Ivanov⁶  · Richard Ghail⁷  · Justin Filiberto⁸  · Jörn Helbert⁴ 

✉ J. Helbert
Joern.Helbert@dlr.de

M.S. Gilmore
mgilmore@wesleyan.edu

¹ Department of Earth and Environmental Sciences, Wesleyan University, Middletown, CT, USA

² Planetary Science Institute, Tucson, AZ, USA

- ³ Department of Astronomy, Mount Holyoke College, South Hadley, MA, USA
- ⁴ German Aerospace Center (DLR) Institute for Planetary Research, Berlin, Germany
- ⁵ Institute for Space Astrophysics and Planetology IAPS, National Institute of Astrophysics, Rome, Italy
- ⁶ Vernadsky Institute of Geochemistry and Analytical Chemistry, Moscow, Russia
- ⁷ Earth Sciences, Royal Holloway, University of London, Egham, UK
- ⁸ NASA Johnson Space Center, Houston, TX, USA